

Figure 3 (A) Specific oscillation at 15–18 Hz generated at the FCD in the superimposed 3D MRI image of Fig. 2C in Patient 1. (B) Top panel: Preoperative superimposed 3D MRI image in Patient 2 showing specific oscillation generated at the superior temporal, middle-frontal gyrus, and inferior frontal gyrus. Bottom panel: Post-operative superimposed 3D MRI image in Patient 2 showing specific oscillation generated at the superior temporal, middle-frontal gyrus, and inferior frontal gyrus. (C) Superimposed 3D MRI image in Patient 3 showing specific oscillation generated in the vicinity of the DNT. (D) Left panel: Preoperative superimposed 3D MRI image in Patient 4 showing broad aberrant oscillation at the left lateral occipital lobe, at the inferior, middle, and superior temporal gyrus, at the angular gyrus, supra-marginal gyrus and the inferior frontal gyrus (red and yellow areas). Right panel: Post-operative superimposed 3D MRI image in Patient 4 showing broad aberrant oscillation at the left angular gyrus and at the inferior frontal gyrus (yellow area). (For interpretation of the references to color in this figure legend, the reader is referred to the web version of the article.)

Based on the FDG-PET findings, the patient underwent left frontal lobe disconnection. The pathology was FCD with dysmorphic neuron and without balloon cells (Palmini type 2A). The patient had remained seizure-free for 8 months and her development improved dramatically.

At age 44 months, 8 months after operation, interictal EEG demonstrated spikes at electrodes Fp1, F3, F7 and fragment polyspikes at electrode F7. The MEG showed residual rhythmic activities at the left frontal–temporal areas. STFT analysis of the moving image indicated that a specific, aber-

rant, 15–20-Hz oscillation was generated at the left superior temporal (Fig. 3B, bottom panel). Subsequently, she had seizure relapse. The ECDs were clustered at the left pars opercularis. Additional resection of the left pars opercularis was performed. The patient has since remained seizure-free for 8 months.

Patient 3

A 15-year-old girl had weekly, but sometimes daily, clusters of seizures. Her development was normal. At 6 years of age, she began to have weekly seizures with deviation of the eyes without loss of consciousness. At 10 years of age, she began to have the sensation of being in an elevator that was falling. Following the aura her head and eyes deviated to the right with loss of consciousness, and in some instances her seizure evolved into right-side clonic seizures. At 14 years of age, the first MRI showed a circumscribed mass of low intensity on T1WI and high intensity on T2WI in the left parietal–occipital regions.

Interictal ^{99m}Tc -ECD-SPECT showed hypoperfusion at the left parietal–occipital areas, which corresponded with the lesion found on MRI. Interictal EEG revealed polyspikes with slow waves at electrodes F3, F4, F7, C3, and C4. The corresponding 204ch MEG showed rhythmic activities in the left frontal and central areas. The ECDs for these spikes were scattered in the anterior vicinity of the MRI lesion. STFT analysis indicated a specific aberrant 20–25-Hz oscillation in the left frontal and central areas. The specific oscillation at 20–25 Hz was generated in the vicinity of the lesion in the moving images (Fig. 3C).

She underwent craniotomy at 16 years of age. The intraoperative ECoG showed 18–25-Hz polyspike bursts at electrodes which were located at the anterior vicinity of the lesion. The frequencies of the MEG oscillation (20–25 Hz) and ECoG polyspike (18–25 Hz) almost corresponded. ECoG polyspikes were located inside the area where the MEG oscillation was depicted by moving images. A total lesionectomy was carried out; the tumor and the gyri involved by the tumor were resected simultaneously.

The tumor was diagnosed as dysembryoplastic neuroepithelial tumor (DNT). One month after the operation, her EEG and MEG showed no fast activity. The patient has been seizure-free for 24 months post-surgery and exhibited no neurological deficits.

Patient 4

A 9-year-old girl had daily seizures. Her seizures initially occurred at 1 month of age with complex partial seizure with motion arrest, loss of consciousness and cyanotic change. Her seizures evolved to daily simple seizures, described as ictal fear and cephalic sensation, and complex partial seizures with motion arrest and autonomic change (cyanotic face) for 3–4 min without remarkable description of dystonic posturing. At 7 years of age, a circumscribed lesion appeared on the MRI in the T1WI at low intensity, in the T2WI and FLAIR at high intensity, in the left temporal parahippocampal gyrus, uncus and hippocampus. At 8 years of age, an EEG performed just before her operation showed independent spikes at the right occipital and left frontal areas, but these were not as intense in the left temporal area where the lesion existed. Furthermore, EEG and

MEG showed intermittent, but prolonged, rhythmic activity at the left frontal and temporal areas. STFT analysis of rhythmic MEG activity during the pre- and post-operative periods demonstrated widespread rhythmic activity in the ipsilateral frontal lobe and in the lateral aspect of the temporal lobe (Fig. 3D, left panel). This rhythmic activity disappeared after the operation and became localized to the left pre- and post-central gyrus (Fig. 3D, right panel).

She underwent an operation at 8 years of age. The intraoperative ECoG showed continuous rhythmic spikes at approximately 20 Hz just before dysplasia resection at the lower area of the left pre- and post-central gyrus and the supra-marginal gyrus. This activity disappeared and became restricted to the left pre-frontal gyrus and supra-marginal gyrus at lower amplitude. One month after surgery, STFT analysis indicated that the oscillation became more restricted and of lower power than in the preoperative MEG (Fig. 3E, right panel).

Discussion

This study indicates that time–frequency analyses using STFT can reveal the distributions of rhythmic fast activity on MEG. This method is useful for pre- and post-surgical evaluation. To improve outcomes from epileptic surgery, it is essential to define the precise location of the epileptogenic zone and the margin of surgical resection by the pre-surgical evaluation. For these purposes, MEG analysis is considered to be a suitable technique, as it offers good temporal and spatial resolution and noninvasive.

We used thiopental for three of the four patients. Thiopental produces fast activity in the beta range (12–30 Hz). However, these fast activities are bilaterally symmetric and developed in a frontal–central area, similar to those appearing during drowsiness (Feshchenko et al., 1997, 2004). The fast activity in our study was generated unilaterally and not in a frontal–central area, thus the fast activity in our study was not attributed to thiopental.

Single dipole modeling has been used mainly to analyze the interictal epileptiform spikes on MEG. Oishi et al. (2006) reported that single clusters of ECDs indicated discrete epileptogenic zones that required complete resection for seizure-free outcome. In the present study, isolated interictal spikes were scarce in Patients 1 and 3, and the ECDs of Patients 1 and 3 were also scattered but not clustered. These ECDs were almost concordant with the high-power area of MEG fast activities, indicating that the SDM localizations were also useful for pre-surgical evaluation in these patients. In contrast, Patient 2 showed few ECDs, due to a scarcity of isolated spikes with sufficient signal-to-noise ratio. The ECDs in Patient 4 were clustered at two remote areas from epileptogenic area at left temporal lobe. These ECDs were discrete from the high-power area of MEG fast activities. ECDs might thereby reflect propagation from the source oscillation. The data obtained from the SDM were, therefore, insufficient for pre-surgical evaluation in our patients.

Ochi et al. (2007) used ECoG to investigate high frequency oscillation (HFO) at the epileptogenic focus and to assess the relationship between the outcome of surgery for epilepsy

and the pattern of HFO. Their findings demonstrated the significant value of preoperative analysis of rhythmic activity. MEG provides higher temporal resolution than EEG and was thus able to show epileptiform discharges more clearly than EEG. For this reason, MEG has the potential to more precisely analyze epileptic rhythmic discharges.

There were several advantages of the MEG findings for pre-surgical evaluation. In our study, epileptic rhythmic activity was demonstrated more clearly by MEG in all patients. Furthermore, the frequency of oscillation appeared faster by MEG than by EEG. For Patients 1, 2, and 4, the EEG showed bilateral fast activity. For Patient 3, EEG showed only a spike or polyspike and a slow wave complex that corresponded to the MEG fast activity. For Patient 2, who was nonlesional on MRI, STFT analysis indicated the epileptic foci, and together with the FDG-PET findings, this information enabled us to plan the disconnection strategy for surgery. For Patient 3, the data enabled us to place the intraoperative ECoG electrodes not only on the lesion, but also at the anterior vicinity of the lesion and source of the fast activity. Similarly, the STFT findings for Patient 4, facilitated placing the ECoG electrodes. STFT analysis of fast activity is thus clearly beneficial for predicting the epileptic foci in patients with poor or several ECDs and for placing the ECoG electrodes.

Our study analyzed the changes in epileptic rhythmic activity before and after surgery for epilepsy and demonstrated the clinical value in predicting the outcome of surgery. For Patient 3, the MEG polyspikes and spikes disappeared following surgery and the patient became seizure-free. For Patients 2 and 4, especially, an aberrant rhythmic oscillation appeared in the remote area of the primary epileptic focus: FCD or DNT. For Patient 4, this rhythmic activity disappeared after the operation. For Patient 2, the MEG polyspikes persisted after surgery and her seizures relapsed. This remote rhythmic activity was defined as secondary epileptogenic focus. In some cases a supplementary operation, such as multiple sub-pial transection, is conducted to treat the secondary focus. Our operative strategy was lesionectomy and we planned further resection according to the seizure outcome and outcome of MEG after the operation. Post-operative MEG showing normal or notably improved aberrant rhythmic oscillation suggests a favorable outcome, whereas post-surgical residual MEG polyspikes may indicate a risk of seizure relapse. Our findings from MEG correlated with seizure outcome. Thus, MEG provides a useful post-surgical evaluation procedure to indicate the need for a secondary operation. In this way, MEG avoids redundant resection and is a safe and noninvasive procedure.

Concerning the correlation between the MEG and ECoG findings, the high-power area of MEG fast activity for Patient 1 with FCD (shown in the red area of the 3D movie; Fig. 3A) and the area of ECoG polyspikes were consistent, with both oscillations colocalizing at the FCD. For Patient 2 with FCD, the ECoG polyspikes were located within the high-power area of MEG fast activity (shown in the red area of the 3D movie; Fig. 3B). For Patient 3 with DNT, the ECoG polyspikes were within the high-power area of MEG fast activity (shown in the red area of the 3D movie; Fig. 3C), and both areas were located near the tumor. For Patient 4 with FCD, the high-power area of MEG fast activity (shown in the yellow area of the 3D movie; Fig. 3D, left panel) was consistent

with the area of ECoG polyspikes. Thus, the MEG fast activity locations demonstrated by STFT colocalized well with the ECoG polyspikes in patients, while MEG areas were rather wider. This could be due to the distance (several cm) between the cortical surface and the MEG sensors, the size of the planar gradiometer sensor, and the distance between sensors.

Guggisberg et al. (2008) showed the clinical value of MEG for the epileptic rhythmic activities in correlation with ECoG. Consistent with the results of previous studies, our findings suggest that STFT of MEG data can depict fast activity that indicate epileptogenic zones associated with FCD and DNT, which are the most significant etiologies of pediatric intractable symptomatic localization-related epilepsy. The excellent post-surgical outcomes achieved for our patients strongly support the predictive value of noninvasive MEG analysis. The rhythmic activities that are closely correlated to the ictogenesis in the cerebral cortex can be demonstrated stereoscopically by noninvasive MEG.

This STFT analysis is limited to patients who have aberrant frequency oscillation like fast activity in our study isolated from the background frequency spectrum. However, unlike ECD and other spatial filtering methods, STFT confers the following advantages. (1) STFT analyzed the original recorded magnetic field data directly. (2) Parameters do not need to be selected arbitrarily to make assumptions about current source and volume conductor, and thus to solve the inverse problem for source localization. (3) STFT indicates the temporal changes. (4) STFT can analyze oscillations that are generated simultaneously over a wide area and with low signal-to-noise ratio.

On the other hand, there were some limitations of this study. First, because the planar gradiometers evaluate the magnetic field just beneath the sensor, STFT could not reflect the depth of source. Second, because of the sensor size of planar gradiometer are 2.8 cm × 2.8 cm and distance between sensor centers is 3.4 cm, there might be a 1–2 cm errors between oscillation sources and projected position of sensor on 3D MRI.

In conclusion, MEG can detect fast activity in symptomatic localization-related epilepsy more clearly and accurately than conventional EEG. STFT reveal the frequency and location of MEG fast activity that could not be analyzed by SDM. The MEG fast activity findings correlated well with the intraoperative ECoG findings and are therefore useful for pre-surgical evaluation. Ascertaining the presence of fast activity after epilepsy surgery could predict the prognosis of seizures. This noninvasive evaluation provides valuable information for pre- and post-surgical evaluations to define surgical strategies for patients with symptomatic localization-related epilepsy induced by circumscribed cortical lesions.

Conflicts of interest

None of the authors has any conflict of interest to disclose.

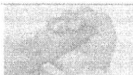
Acknowledgments

We thank Prof. Tadashi Ariga of the Department of Pediatrics, Hokkaido University Graduate School of Medicine,

for his valuable editorial opinion. In addition, we thank Dr. Akiyoshi Kakita of the Brain Research Institute, Niigata University for pathology diagnoses. We confirm that we have read the Journal's position on issues involved in ethical publication and affirm that this report is consistent with those guidelines. This work was supported in part by Grants-in-aid for Scientific Research (18591136) from the Japan Society of the Promotion of Science, and the Japan Epilepsy Research Foundation.

References

- Bonati, L.H., Naegelin, Y., Wieser, H.G., Fuhr, P., Ruegg, S., 2006. Beta activity in status epilepticus. *Epilepsia* 47, 207–210.
- Bosnyakova, D., Gabova, A., Kuznetsova, G., Obukhov, Y., Midzyanovskaya, I., Salonin, D., van Rijn, C., Coenen, A., Tuomisto, L., van Luijckeloo, G., 2006. Time–frequency analysis of spike-wave discharges using a modified wavelet transform. *J. Neurosci. Methods* 154, 80–88.
- Ebersol, J.S., 1997. Magnetoencephalography/magnetic source imaging in the assessment of patients with epilepsy. *Epilepsia* 38 (Suppl. 4), S1–S5.
- Feshchenko, V.A., Veselis, R.A., Reinsel, R.A., 1997. Comparison of the EEG effects of midazolam, thiopental, and propofol: the role of underlying oscillatory systems. *Neuropsychobiology* 35, 211–220.
- Feshchenko, V.A., Veselis, R.A., Reinsel, R.A., 2004. Propofol-induced alpha rhythm. *Neuropsychobiology* 50, 257–266.
- Gambardella, A., Palmieri, A., Andermann, F., Dubeau, F., Da Costa, J.C., Quesney, L.E., Andermann, E., Livier, A., 1996. Usefulness of focal rhythmic discharges on scalp EEG of patients with focal cortical dysplasia and intractable epilepsy. *Electroencephalogr. Clin. Neurophysiol.* 98, 243–249.
- Grosse, P., Cassidy, M.J., Brown, P., 2002. EEG-EMG, MEG-EMG and EMG-EMG frequency analysis: physiological principles and clinical applications. *Clin. Neurophysiol.* 113, 1523–1531.
- Guggisberg, A.G., Kirsch, H.E., Mantle, M.M., Barbaro, N.M., Nagarajan, S.S., 2008. Fast oscillations associated with interictal spikes localize the epileptogenic zone in patients with partial epilepsy. *Neuroimage* 39, 661–668.
- Hämäläinen, M.S., Hari, R., Ilmoniemi, R., Knuutila, J., Lounasmaa, O.V., 1993. Magnetoencephalography: theory, instrumentation, and applications to noninvasive studies of the working human brain. *Rev. Mod. Phys.* 65, 413–497.
- Haykin, S., Racine, R.J., Xu, Y., Chapman, C.A., 1996. Monitoring neuronal oscillations and signal transmissions between cortical regions using time–frequency analysis of electroencephalographic activity. *Proc. IEEE* 84, 1295–1301.
- Hooshmand, H., Morganroth, R., Corredor, C., 1980. Significance of focal and lateralized beta activity in the EEG. *Clin. Electroencephalogr.* 11, 140–144.
- Iwasaki, M., Pestana, E., Burgess, R.C., Lüders, H.O., Shamoto, H., Nakasato, N., 2005. Detection of epileptiform activity by human interpreters: blinded comparison between electroencephalography and magnetoencephalography. *Epilepsia* 46, 59–68.
- Kiyimik, M.K., Güler, I., Dizibüyük, A., Akin, M., 2005. Comparison of STFT and wavelet transform methods in determining epileptic seizure activity in EEG signals for real-time application. *Comput. Biol. Med.* 35, 603–616.
- Lee, S.K., Kim, J.Y., Hong, K.S., Nam, H.W., Park, S.H., Chung, C.K., 2000. The clinical usefulness of ictal surface EEG in neocortical epilepsy. *Epilepsia* 41, 1450–1455.
- Ochi, A., Otsubo, H., Donner, E.J., Elliott, I., Iwata, R., Funaki, T., Akizuki, Y., Akiyama, T., Imai, K., Rutka, J.T., Snead 3rd, O.C., 2007. Dynamic changes of ictal high-frequency oscillations in neocortical epilepsy: using multiple band frequency analysis. *Epilepsia* 48, 286–296.
- Oishi, M., Kameyama, S., Masuda, H., Tohyama, J., Kanazawa, O., Sasagawa, M., Otsubo, H., 2006. Single and multiple clusters of magnetoencephalographic dipoles in neocortical epilepsy: significance in characterizing the epileptogenic zone. *Epilepsia* 47, 355–364.
- Oppenheim, A., Schaffer, R.W., 1999. *Discrete-Time Signal Processing*. Prentice Hall, Englewood Cliffs, New Jersey.
- Park, S.A., Lim, S.R., Kim, G.S., Heo, K., Park, S.C., Chang, J.W., Chung, S.S., Choi, J.U., Kim, T.S., Lee, B.I., 2002. Ictal electrocorticographic findings related with surgical outcomes in nonlesional neocortical epilepsy. *Epilepsy Res.* 48, 199–206.
- Talairach, J., Bancaud, J., Bonis, A., Szikla, G., Trottier, S., Vignal, J.P., Chauvel, P., Munari, C., Chodkiewicz, J.P., 1992. Surgical therapy for frontal epilepsies. *Adv. Neurol.* 57, 707–732.
- Worrell, G.A., So, E.L., Kazemi, J., O'Brien, T.J., Mosewich, R.K., Cascino, G.D., Meyer, F.B., Marsh, W.R., 2002. Focal ictal beta discharge on scalp EEG predicts excellent outcome of frontal lobe epilepsy surgery. *Epilepsia* 43, 277–282.



and 83%, respectively.¹ However, patients presenting with an advanced stage of adult WT still show a poor outcome. In a recent NWTs retrospective report, OS (with a mean observation time of 54 months) was only 20% for stage IV adult WT.⁷

The present patient initially presented with highly extensive disease, which was cured with multimodal therapy based on pediatric strategy. Because the patient's hematological toxicities were always serious, the interval between chemotherapy was thus prolonged. In addition, we also decided to use the minimum required radiation dosage and PBSC rescue. Furthermore, the patient's neurotoxicity secondary to vincristine was also serious, thus requiring the use of special equipment.

This case demonstrated that WT observed in the adolescent and adult population, even when identified at an advanced stage, appears to be curable if multimodal treatment according to the established pediatric strategy is effectively performed. However, toxicity such as hematological toxicity and neuropathy may develop at a higher incidence and at a more severe grade.^{1,2} In this case the PBSC rescue may not have been needed, however this method should nevertheless be considered in patients presenting with severe hematological toxicity. Kalapurakal *et al.* pointed out the risk of veno-occlusive disease associated with an overdosage of ACD in adult patients.² Therefore, such toxicities should be closely monitored in adult patients with WT. Moreover, prospective trials in both adolescent and adult patients with WT are

warranted in order to establish the appropriate dosages and optimal schedule of chemotherapy, as well as to determine the ideal sequence and effective design of local treatments and supportive care.

References

- 1 Reinhard H, Aliani S, Ruebe C *et al.* Wilms' tumor in adults: results of the Society of Pediatric Oncology (SIOP) 93-01/ Society for Pediatric Oncology and Hematology (GPOH) study. *J. Clin. Oncol.* 2004; **22**: 4500–6.
- 2 Kalapurakal JA, Nan B, Norkool P *et al.* Treatment outcomes in adults with favorable histologic type Wilms tumor. *Int. J. Radiat. Oncol. Biol. Phys.* 2004; **60**: 1379–84.
- 3 Arrigo S, Beckwith JB, Sharples K *et al.* Better survival after combined modality care for adults with Wilms' tumor. A report from National Wilms' Tumor Study. *Cancer* 1990; **66**: 827–30.
- 4 Kaste SC, Dome JS, Babyn PS *et al.* Wilms tumor: prognostic factors, staging, therapy and late effects. *Pediatr. Radiol.* 2008; **38**: 2–17.
- 5 Pizzo PA, Poplack DG, eds. *Principles and Practice of Pediatric Oncology*, 5th edn. Lipponcott Williams and Wilkins, Philadelphia, PA, 2006; 905–32.
- 6 Byrd RL, Evans AE, D'Angio GJ. Adult Wilms's tumor: effect of combined therapy on survival. *J. Urol.* **982**(27): 648–51.
- 7 Izawa JI, Al-Omar M, Winkvist E *et al.* Prognostic variables in adult Wilms tumor. *Can. J. Surg.* 2008; **51**: 252–6.

Vaccine-associated paralytic poliomyelitis in a non-immunocompromised infant

Naoko Asahina,¹ Yukiko Matsunami,² Keitaro Sueda,¹ Hideaki Shiraishi¹ and Shinji Saitoh¹

¹Department of Pediatrics, Hokkaido University Graduate School of Medicine and ²Department of Pediatrics, KKR Sapporo Medical Center, Sapporo, Japan

Key words oral poliovirus vaccine, poliomyelitis, primary immunodeficiencies, tissue injury, vaccine-associated paralytic poliomyelitis.

Oral poliovirus vaccine (OPV) was introduced in Japan in 1961 and it has become a routine immunization for infants since 1964. During the 1960s, the widespread use of OPV led to a dramatic decrease in the number of patients contracting poliomyelitis. Since 1981, no poliomyelitis cases caused by wild poliovirus have been reported in Japan.¹ Live virus vaccination, however, is associated with the serious consequence of vaccine-associated paralytic poliomyelitis (VAPP). In 2002, the World Health Organization estimated that between 250 and 500 cases of VAPP occur

every year due to the use of OPV in routine childhood immunization programs around the world.² Although VAPP can occur in healthy recipients or their close contacts, persons with primary immunodeficiencies have a much higher risk of the disease.^{3,4}

In Japan, the overall risk for recipient and contact VAPP has been reported as one case in every 2 million doses given, while the risk of recipient VAPP and recipient VAPP following the first OPV dose is one in every 3.7 million doses and one in every 2.3 million doses given, respectively.⁵

In this study, we report a case of VAPP in an infant who did not have any obvious immunodeficiency.

Case report

A 7-month-old male infant of healthy parents was presented with a high fever of 39°C and a perianal abscess, 15 days after his first

Correspondence: Shinji Saitoh, MD PhD, Department of Pediatrics, Hokkaido University Graduate School of Medicine, North 15, West 7, Kita-ku, Sapporo 060-8638, Japan. Email: ss11@med.hokudai.ac.jp

Received 23 May 2009; revised 8 January 2010; accepted 29 January 2010.

doi: 10.1111/j.1442-200X.2010.03132.x

OPV. His birth and developmental history were normal. He was hospitalized and his perianal abscess was treated with intravenous antibiotics and dissection of the abscess. Although his perianal abscess resolved, his high fever continued. His crying became weaker and he suddenly developed a flaccid paralysis of his extremities and trunk on day 5 of hospitalization. Brain and sagittal spinal magnetic resonance imaging (MRI) did not show any obvious abnormalities (an axial MRI view of the spine was not performed). A lumbar puncture was performed and the cerebrospinal fluid (CSF) showed 7 mononuclear cells/mm³, 91 mg/dL protein, and 49 mg/dL glucose. He received i.v. γ -globulin therapy (2 g/kg/dose). The flaccid paralysis of his upper limbs and trunk improved on day 10, however paralysis of both lower limbs, but predominantly the right, continued. Right patellar and Achilles tendon reflexes were not detectable and left patellar and Achilles tendon reflexes were diminished. Plantar reflexes were absent. Sensory abnormalities were not detectable, and bladder and rectal dysfunction were not noted.

On day 45, his CSF showed 21 mononuclear cells/mm³, 28 mg/dL protein, and 49 mg/dL glucose. Polymerase chain reac-

Table 1 Serum poliovirus-neutralizing antibody titer of the patient at 40 days and 10 months after the onset of illness

Virus type	40 days	10 months
PV type 1	1 : 16	<1 : 4
PV type 2	1 : 16	1 : 4
PV type 3	1 : 32	1 : 4

PV, poliovirus.

tion (PCR) for adenovirus, enteroviruses and herpes simplex viruses in the CSF was negative. The neutralizing antibody titer for poliovirus in the CSF was also negative.

All biochemical tests were within normal limits. In the serum, neutralizing antibody titers for poliovirus type 1, 2, and 3 were 1 : 16, 1 : 16, and 1 : 32, respectively. Ten months after onset, the corresponding antibody titers were negative, 1 : 4, and 1 : 4, respectively (Table 1). Detailed investigation of his immune status showed no abnormalities, both at the time of admission and 10 months later. White blood cell, neutrophil and lymphocyte counts were 18 300, 12 900 and 4026 cells/ μ L, respectively, and

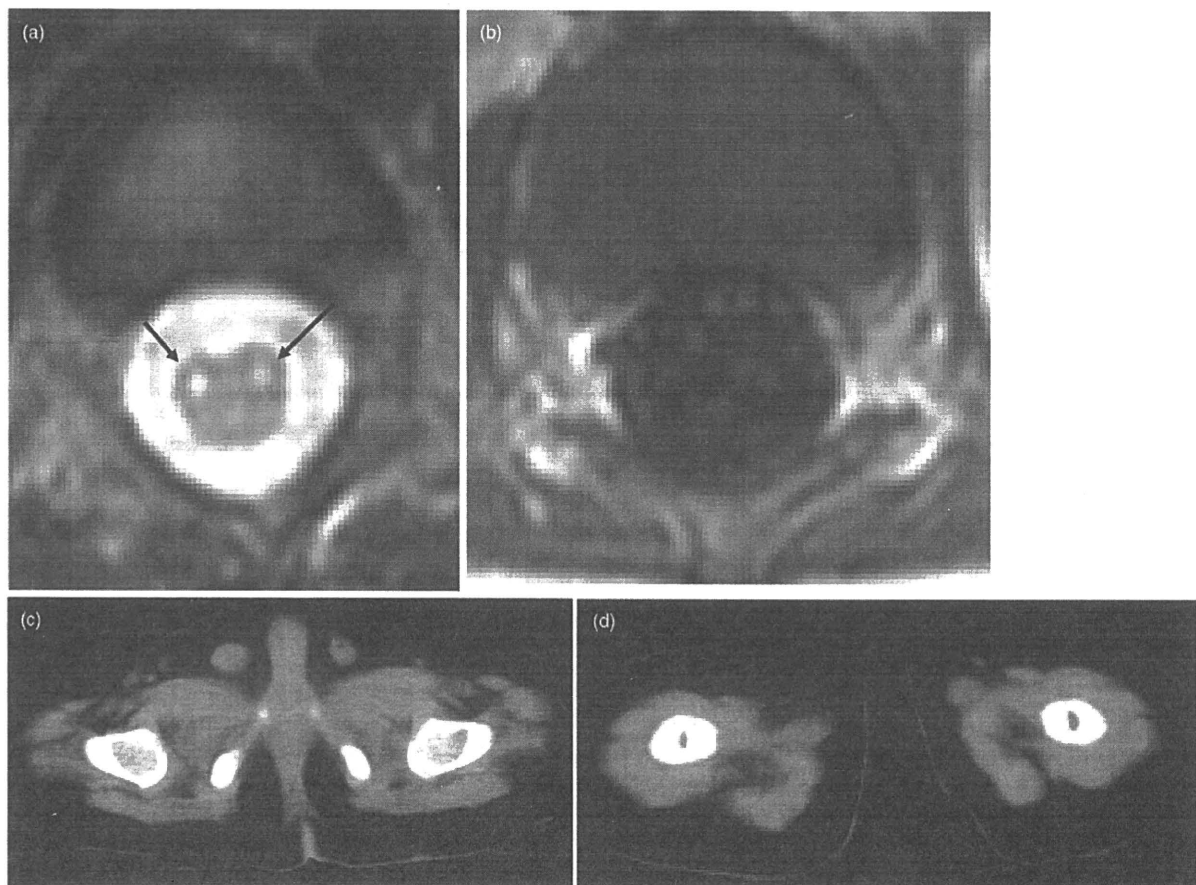


Fig. 1 Magnetic resonance imaging (MRI) and computed tomography (CT) images taken on day 39 of illness. (a) Axial image of T2-weighted MRI demonstrating bilateral high-intensity signals (arrows) in the anterior spinal cord at the level of T11. (b) Axial image of gadolinium-enhanced T1-weighted MRI demonstrating an enhanced ventral cauda equina. (c) CT images showing severe bilateral muscle atrophy in the gluteus and (d) femoral muscles.

his immunoglobulin (Ig) G level was 685 mg/dL at the time of admission. Ten months later, white blood cell, neutrophil and lymphocyte counts were 7400, 2146 and 4144 cells/ μ L, respectively; cluster of differentiation (CD)3-, CD4-, CD8-, CD19- and human leukocyte antigen (HLA)-DR-positive lymphocyte counts were 3037, 2076, 804, 820 and 887 cells/ μ L, respectively; and his IgG level was 806 mg/dL. Poliovirus was isolated from the feces on days 42 and 45 and was identified as poliovirus type 3 in a virus-neutralization test; it was later found to be a Sabin-3 (VP1 region)/Sabin-1 (3D region) recombinant vaccine strain because its serotype and intratypic differentiation were similar to OPV by the PCR-restriction fragment length polymorphism method and sequencing.⁶

T2-weighted MRI (axial section) on day 39 demonstrated a high-intensity signal bilaterally in the anterior horn of the spinal cord at the level of T11 and T12 (Fig. 1a). The sagittal view of the spinal MRI did not show any obvious abnormalities. Gadolinium-enhanced T1-weighted MRI showed an enhanced signal in the ventral cauda equina (Fig. 1b). Computed tomography on day 39 showed severe atrophy of the gluteus and femoral muscles bilaterally (Fig. 1c,d). Conduction velocities of the medial nerves were within normal limits, but conduction velocities of the tibial nerves were decreased (Fig. 2).

The infant underwent rehabilitation and physical therapy, but he still has severe motor impairment with hypotonia and weakness of the lower limbs at 2 years of age. He can stand using lower limb orthoses, but cannot walk; he also has severe scoliosis.

Discussion

Poliovirus is an enterovirus transmitted mainly by fecal-oral contamination. After poliovirus infection, most people are asymptomatic or have a non-specific illness including mild fever, malaise, headache, sore throat and gastrointestinal upset. Among those who have a non-specific illness, 1–2% of individuals progress to paralytic disease. The paralysis evolves and fixes rapidly during the fever, and often leaves asymmetrical muscle atrophy, but without sensory, bladder or rectal dysfunction. Although poliovirus can involve any structure of the nervous system, the virus tends to affect the larger motor neurons, particularly those of the anterior horn of the spinal cord and the motor nuclei of the medulla. In the acute to subacute phase, the ventral horn cells are characterized by a severe inflammation, neuronophagia, active gliosis and destruction of the anterior horn cells. This correlates with the abnormalities seen on spinal MRI.⁷ In the present case, the abnormality could not be detected on the sagittal section of the spinal MRI, although the lesion existed in the anterior horn cells at the onset of paralysis.

Cases of VAPP have been reported in many countries using OPV.² In Japan and other countries VAPP is usually associated with polio virus type 2 and 3, but rarely type 1. The clinical course of VAPP is similar to that of wild poliovirus, so it is difficult to distinguish between VAPP and poliomyelitis caused by the wild virus. Previous reports indicate that persons with primary immunodeficiencies have a much higher risk of the disease.^{3,4} The present case of recipient VAPP following the first OPV dose involved the type 3 vaccine virus, but we were unable

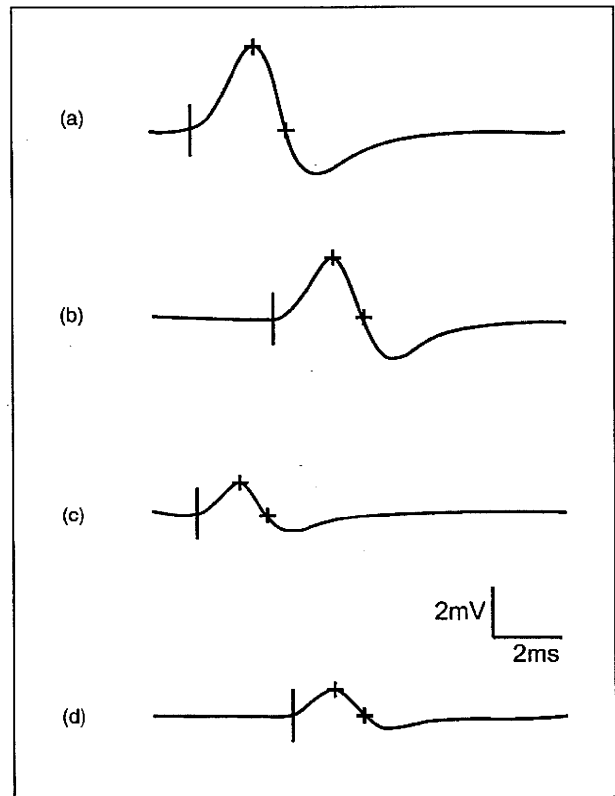


Fig. 2 Motor conduction velocities in the tibial nerve on day 40 of illness showing a reduction in the right side (left, 35.4 m/s; right, 28.5 m/s). (a) Left ankle stimulation; amplitude 4.3 mV. (b) Left knee stimulation; amplitude 3.2 mV. (c) Right ankle stimulation; amplitude 1.7 mV. (d) Right knee stimulation; amplitude 1.3 mV.

to detect any obvious immunodeficiencies in the infant. We considered that his serum-neutralizing antibody titer for poliovirus on day 40 was raised under the influence of intravenous γ -globulin therapy besides vaccination. After ten months, his antibody titer for poliovirus type 2 and 3 had decreased, but was maintained at 1 : 4 and the immunity persisted. His antibody titer for poliovirus type 1 became negative after ten months suggesting that immunity was not acquired from a single vaccination.

Strebel *et al.*⁸ reported that the risk of VAPP increased with tissue injury, such as intramuscular injection, within one month of immunization with OPV. It is also suggested that skeletal muscle injury induces retrograde axonal transport of poliovirus and thereby facilitates viral invasion of the central nervous system and progression of spinal cord damage.⁹ Bosley *et al.*¹⁰ reported an infant with VAPP who had a perianal abscess simultaneously. In our case, when the infant was given OPV, he might have had a perianal injury and he was treated for his perianal abscess just before his paralytic illness appeared. The perianal abscess itself, or dissection of the abscess, may have caused skeletal muscle injury and increased the risk of VAPP. We therefore consider that the perianal abscess was an important factor in the development of VAPP and influenced the pathogenesis of the disease.

It is apparent that VAPP occurs constantly in countries where the live virus polio vaccine is used, as adverse reactions to OPV in healthy infants without any obvious immunodeficiencies can occur, as in our case. In 2000, the American Academy of Pediatrics changed their policy to recommend only inactivated poliovirus vaccine (IPV) for routine childhood immunization, because they considered VAPP would not be eliminated unless the use of OPV was stopped.¹¹ Recently, some countries including the USA and Germany have changed their national policies to recommend vaccination with IPV alone instead of OPV.¹² Therefore, we believe that the introduction of IPV should be seriously considered in Japan.

References

- Yoneyama T, Karoji Y, Watanabe K, Tsuchiya M, Nakano M, Miyamura T. Surveillance of poliovirus-isolates in Japan, 1999. *Jpn. J. Infect. Dis.* 2000; **53**: 90-1.
- Global Commission for the Certification of the Eradication of Poliomyelitis. *Meeting (2002; Geneva, Switzerland). Report of the Interim Meeting of the Technical Consultative Group (TCG) on the Global Eradication of Poliomyelitis, Geneva, 13-14 November 2002.* World Health Organization, Geneva, 2003.
- Parvaneh N, Shahmahmoudi S, Tabatabaie H *et al.* Vaccine-associated paralytic poliomyelitis in a patient with MHC class II deficiency. *J. Clin. Virol.* 2007; **39**: 145-8.
- Manishi S, Shahmahmoudi S, Tabatabaie H *et al.* Novel *BTK* mutation presenting with vaccine-associated paralytic poliomyelitis. *Eur. J. Pediatr.* 2008; **167**: 1335-8.
- Hao L, Toyokawa S, Kobayashi Y. Poisson-model analysis of the risk of vaccine-associated paralytic poliomyelitis in Japan between 1971 and 2000. *Jpn. J. Infect. Dis.* 2008; **61**: 100-3.
- Balanant J, Guillot S, Candrea A, Delpyroux F, Crainic R. The natural genomic variability of poliovirus analyzed by a restriction fragment length polymorphism assay. *Virology* 1991; **184**: 645-54.
- Kornreich L, Dagan O, Grunebaum M. MRI in acute poliomyelitis. *Neuroradiology* 1996; **38**: 371-2.
- Strebel PM, Ion-Nedelcu N, Baughman AL, Sutter RW, Cochi SL. Intramuscular injections within 30 days of immunization with oral poliovirus vaccine – a risk factor for vaccine associated paralytic poliomyelitis. *N. Engl. J. Med.* 1995; **332**: 500-6.
- Gromeier M, Wimmer E. Mechanism of injury-provoked poliomyelitis. *J. Virol.* 1998; **72**: 5056-60.
- Bosley AR, Speirs G, Markham NI. Provocation poliomyelitis: vaccine associated paralytic poliomyelitis related to a rectal abscess in an infant. *J. Infect.* 2003; **47**: 82-4.
- American Academy of Pediatrics, Committee on Infectious Diseases. Prevention of poliomyelitis: recommendations for use of only inactivated poliovirus vaccine for routine immunization. *Pediatrics* 1999; **104**: 1404-6.
- Alexander LN, Seward JF, Santibanez TA *et al.* Vaccine policy changes and epidemiology of poliomyelitis in the United States. *JAMA* 2004; **292**: 1696-701.

Conservative treatment of a large post-infectious pneumatocele

Leon Joseph,¹ Sarit Shahroor,² Drora Fisher,³ Shmuel Goldberg¹ and Elie Picard¹

¹Pediatric Pulmonology Unit, ²Pediatric Intensive Care Unit, ³Pediatric Radiology Department, Shaare Zedek Medical Center, Affiliated with the Hebrew University-Hadassah Medical School, Jerusalem, Israel

Key words conservative management, necrotizing pneumonia, pneumatocele.

A pneumatocele (PC) is an air-filled cyst within the lung parenchyma that is usually thin-walled. It is most commonly seen in children secondary to a severe pulmonary infection sometimes complicated by pleural effusion.¹ The airways undergo necrosis and the resultant cystic lesion is connected to the bronchial tree. This connection is unidirectional causing hyperinflation of the cyst. In the past, the most common pathogen associated with PC was *Staphylococcus aureus*, but recently there has been an increase in the incidence of *Streptococcus-pneumoniae*-associated PC.^{2,3} In two recent series of pneumococcal pneumonia, PC developed in 7%³ and 18%³ of the patients, respectively.

There is no fully accepted consensus for treatment of PC. In 1983, 12 cases of pneumatocele were reported with two patients who died from progressive respiratory failure with no apparent

attempt to reduce the size of the PC.⁴ In 1996, the first report of computed-tomography-(CT)-guided intrapulmonary drainage of five patients with PC had good results.⁵ A recent paper by Imamoglu *et al.*⁶ proposed a protocol for treating PC. According to their criteria, PC larger than 50% of the hemithorax, those that cause severe atelectasis, those that have persistent symptoms, or are poorly tolerated during follow up, should be treated. Using "thin wall" as another indication for treatment, they recommend image-(CT)-guided catheter drainage (IGCD) as having good results in their series for all those drained who had thin-walled PC. However, two cases in their series that had long-standing thick-walled PC were not cured after catheter drainage and underwent surgical resection.

Although our case fulfilled the above criteria for drainage, it was successfully treated conservatively. Our Institutional Review Board waived the need for consent.

Case Report

A 14-month-old male infant presented to our emergency department with fever and cough. A full examination and blood count

Correspondence: Elie Picard, MD, Pediatric Respiratory Unit, Shaare Zedek Medical Center, Jerusalem 91031, Israel. Email: picard@szmc.org.il

Received 19 November 2009; revised n/a; accepted 1 February 2010.

doi: 10.1111/j.1442-200X.2010.03137.x

MERRF/MELAS overlap syndrome: a double pathogenic mutation in mitochondrial tRNA genes

M Nakamura,¹ I Yabe,¹ A Sudo,² K Hosoki,² H Yaguchi,¹ S Saitoh,² H Sasaki¹

¹Department of Neurology, Hokkaido University Graduate School of Medicine, Sapporo, Japan

²Department of Pediatrics, Hokkaido University Graduate School of Medicine, Sapporo, Japan

Correspondence to

Ichiro Yabe, Department of Neurology, Hokkaido University Graduate School of Medicine, N15W7, Kita-ku, Sapporo 060-8638, Japan; yabe@med.hokudai.ac.jp

MN & IY contributed equally to this study.

Received 31 October 2009
Accepted 11 January 2010
Published Online First
7 July 2010

ABSTRACT

Background Myoclonic epilepsy with ragged-red fibres (MERRF) and mitochondrial encephalopathy, lactic acidosis and stroke-like episodes (MELAS) are established phenotypes of mitochondrial encephalomyopathy. The m.8356T>C transition in the mitochondrial tRNA^{Lys} gene is a pathogenic mutation of MERRF. The m.3243A>G transition in the mitochondrial tRNA^{Leu} gene is detected in most MELAS patients. Although previous analyses of double mutations in mitochondrial DNA (mtDNA) were useful for discussing their nature, many unsolved questions remain.

Objective To describe the clinical and genetic features of a family with the above mtDNA double-point mutations and discuss the role of double mtDNA mutations in diverse clinical features in the family.

Patients and methods The proband was a 23-year-old woman with MERRF harbouring m.8356T>C and m.3243A>G transitions in mitochondrial tRNA genes. We assessed clinical aspects of her and those of her three relatives and performed mutation analyses on their mtDNA.

Results Phenotypes of the four patients were MERRF, MERRF/MELAS overlap syndrome and asymptomatic carrier. We hypothesise that the course of the phenotype of this family begins with MERRF and is followed by MELAS. This double mutation was heteroplasmic in blood of all four patients but with different rates in each patient, while m.8356T>C appeared homoplasmic and m.3243A>G was heteroplasmic in muscle of the two examined cases. No other mutations were detected in the total mtDNA sequence in this family.

Conclusions This is the first reported case of a double-point mutation in mtDNA, both of which were heteroplasmic and pathogenic for the established phenotypes.

The concept of myoclonic epilepsy with ragged-red fibres (MERRF) was first proposed in 1980 and has been established as one of the phenotypes of mitochondrial encephalomyopathy.¹ It is maternally inherited, and patients express myoclonus, myoclonic or generalised convulsions, cerebellar ataxia and myopathy with ragged-red fibres.² In 1990, the most common pathogenic mutation, m.8344A>G transition, in the mitochondrial tRNA^{Lys} gene was reported,³ and report of a second pathogenic mutation, m.8356T>C transition, in the mitochondrial tRNA^{Lys} gene followed in 1992.⁴ The first report of the m.8356T>C transition indicated a pure MERRF expression⁴; however, subsequent reports revealed that patients, with or without MERRF symptoms, of the families with this mutation, frequently showed migraine, stroke-like episodes and strongly succinate

dehydrogenase-reactive vessels (SSVs) in muscle pathology, which are typical for another phenotype of mitochondrial encephalomyopathy; mitochondrial myopathy, encephalopathy, lactic acidosis and stroke-like episodes (MELAS).^{5,6} It was speculated that the m.8356T>C transition might occur in patients with some of the expressions of MELAS, such as migraine, stroke-like episodes and SSVs; however, the mechanism by which various expressions typical for two distinct phenotypes might occur in patients with only this point mutation in mitochondrial DNA (mtDNA) has not been clarified.^{5,6}

The concept of MELAS was proposed in 1984, also as one of the phenotypes of mitochondrial encephalomyopathy.⁷ This entity was maternally inherited and characterised by stroke-like episodes, episodic headache and vomiting, seizures, dementia, lactic acidosis, skeletal myopathy, short stature and as being with or without MERRF symptoms.⁷ The first pathogenic mutation, the m.3243A>G transition in the mitochondrial tRNA^{Leu} gene, was reported in 1990.⁸ Moreover, it was revealed that most of the patients with MELAS had this mutation as a primary cause of the disease.⁹ On the other hand, there were several reports of patients with an m.3243A>G transition, who also expressed features typical of phenotypes of mitochondrial encephalomyopathy other than MELAS, such as MERRF,^{10,11} MERRF/MELAS overlap syndrome,^{12,13} progressive external ophthalmoplegia (PEO) and MERRF/PEO overlap syndrome,¹⁴ suggesting that the m.3243A>G transition was potentially indicative of a broad expressive spectrum. However, what determined the range of expression in each patient had not been resolved.^{10–14}

There are reports of rare families with mitochondrial encephalomyopathy, possessing double-point mutations in mtDNA.^{15–22} Some of these consist of two mutations reported to separately express the same^{15,18,20,22} or different^{17,19,21} distinct phenotypes, and others consist of one mutation of a well-known pathogenesis and one mutation of unknown effect.¹⁶ It is speculated that in some families, only one of the mutations expresses a phenotype,^{16,17} that each mutation expresses different phenotypes in a given family¹⁹ and both mutations act synergistically to express one phenotype in other families.^{18,21,22} These double mtDNA mutations might be the key to resolving the mechanisms underlying the formation of threshold effects. However, these issues have yet to be resolved, presumably due in part to the various combinations of established phenotypes and mutational expressions in each of the families mentioned above.

Original article

We encountered a family with the double mutation, m.8356T>C and m.3243A>G. Individual family members expressed MERRF, MERRF/MELAS overlap syndrome and other minor complications compatible with symptoms derived from mitochondrial dysfunctions. Because the various family members express potential phenotypes known to be caused by these two mtDNA mutations, they were considered advantageous for discussing the relationship between phenotypes and genetic effects. We had a chance to examine four members of this family and tried to clarify the expression and the role of mtDNA point mutations.

PATIENTS AND METHODS

Patients

The pedigree of the family we will discuss is shown in figure 1. We first met patient III-1 (proband). She was introduced to us from another institution, diagnosed with myoclonic epilepsy. An interview of her and her mother (II-1) revealed that they had a familial history of mitochondrial encephalomyopathy (II-2; maternal aunt of the proband). We subsequently discovered that one of our colleagues had examined II-2 and had identified mtDNA double-point mutation (m.8356T>C and m.3243A>G) by a commercial-based (SRL Inc.) analysis of common mtDNA mutations and that her muscle specimen had been preserved in our institution. Another patient of this family (III-6; cousin of the proband) was introduced to us from another institution, also diagnosed with myoclonic epilepsy. Thus, the main participants of this study are these four cases: II-1 (mother), II-2 (maternal aunt), III-1 (proband) and III-6 (cousin). This pedigree contains other cases with hearing loss (I-1), hearing loss and mental retardation (III-5) and sudden death at one year of age (III-7). However, as we did not encounter these family members, we have no further information about them.

We conducted clinical (physical, neurological, laboratory and radiological) examinations of II-1, III-1 and III-6 as far as we could. Clinical information of II-2 was gained from medical records. Histochemical analysis of muscle was conducted for II-2 and III-1. Genetic analyses of mtDNA from blood and/or muscle was conducted in all four cases.

Report of cases

III-1: the proband

A 17-year-old woman with bilateral sensorineural deafness developed a generalised clonic convulsion; she was diagnosed with myoclonic epilepsy 1 year later. Sodium valproate had been effective for preventing relapses of epileptic seizures. She was introduced to us at age 23 because her maternal aunt (II-2) was diagnosed with MELAS. She exhibited a slightly short stature (154 cm) and definitely low body weight (36 kg). She did not complain of either episodic headache or nausea. Neurological

examinations revealed deafness, slurred speech, weakness of bilateral quadriceps, and limb and truncal ataxia. By conversation, we were impressed that although she was somewhat childish for her age, her cognitive function was preserved. Her visual acuity and field were not disturbed. External ophthalmoplegia was not observed. Serum chemistry examinations detected no elevations in lactate, creatine kinase, transaminases, lactate dehydrogenase, amylase, haemoglobin A_{1c} and creatinine. Blood hormonal evaluations of pituitary gland (ACTH, TSH, LH, FSH, GH, and prolactin), thyroid (FT3, FT4), adrenal cortex (cortisol) and genitals (oestradiol) were normal. Elevated lactate was detected in cerebrospinal fluid (35.3 mg/dl; normal <20.0 mg/dl). A CT scan of the trunk showed no abnormal forms of the organs in chest and abdomen. Transthoracic ultrasonic cardiography did not reveal cardiomyopathy. A brain MRI scan showed diffuse mild brain atrophy without focal lesions. Electroencephalography (EEG) showed bilateral slow waves. A muscle biopsy of the left *rectus femoris* revealed fibre size variability, scattered ragged-red fibres (RRFs) and SSVs (figure 2A). Cytochrome c oxidase defects were detected in occasional fibres (focal COX deficiency), also among RRFs (figure 2B). Most of the SSVs (approximately 80%) possessed COX activity.

II-2: maternal aunt of III-1

The proband's maternal aunt had bilateral sensorineural deafness and progressive myoclonic epilepsy when she was 26 years old. At age 38, she developed stroke-like episodes with headache, truncal instability and convulsion; she exhibited emaciation (stature 157 cm, body weight 38 kg). Neurological examinations revealed aphasia, right hemianopsia and cerebellar ataxia. A brain MRI scan showed a large lesion in the left cerebral hemisphere (figure 3). Elevated lactate (34.6 mg/dl; normal <16.0 mg/dl) and impaired glucose tolerance (data not shown) were detected in serum. A muscle biopsy of the left *rectus femoris* showed fibre size variability, RRFs, focal COX deficiency and SSVs (figure 2C,E). Some SSVs (approximately 40%) lacked COX activity (figure 2C-F), and occasional RRFs also lacked COX activities. A stroke-like episode relapsed with disturbed consciousness at age 45, and the patient died of renal and heart failure 1 year later.

III-6: cousin of III-1

A female cousin of the proband developed slurred speech, dysmetria of all four extremities and truncal instability at age 18. After a few months, myoclonic jerks of the upper extremities often appeared, followed by generalised clonic convulsions. Her stature and body weight were in the normal range. She had neither deafness nor a history of episodic headache and nausea. Neurological findings revealed a slight cerebellar ataxia of the trunk and limbs, transient myoclonus of the upper extremities and an episode of generalised convulsion. She appeared childish during conversation, but intellectual ability was normal. Her visual acuity and field were intact. External ophthalmoplegia was not observed. Serum creatine kinase, transaminases, lactate dehydrogenase, amylase, haemoglobin A_{1c} and creatinine were within normal limits, but lactate was elevated (16.4 mg/dl; normal <16.0 mg/dl). Transthoracic ultrasonic cardiography indicated normal wall motion of the heart. A brain MRI showed no definite abnormalities. She showed left dominant spike-and-waves on an EEG and was diagnosed with myoclonic epilepsy at age 19. For about 1.5 years, myoclonic epilepsy was well controlled with carbamazepine; however, at age 21, the frequency of the epileptic seizures increased. Despite changes to,

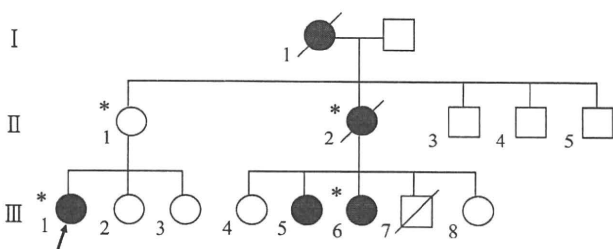
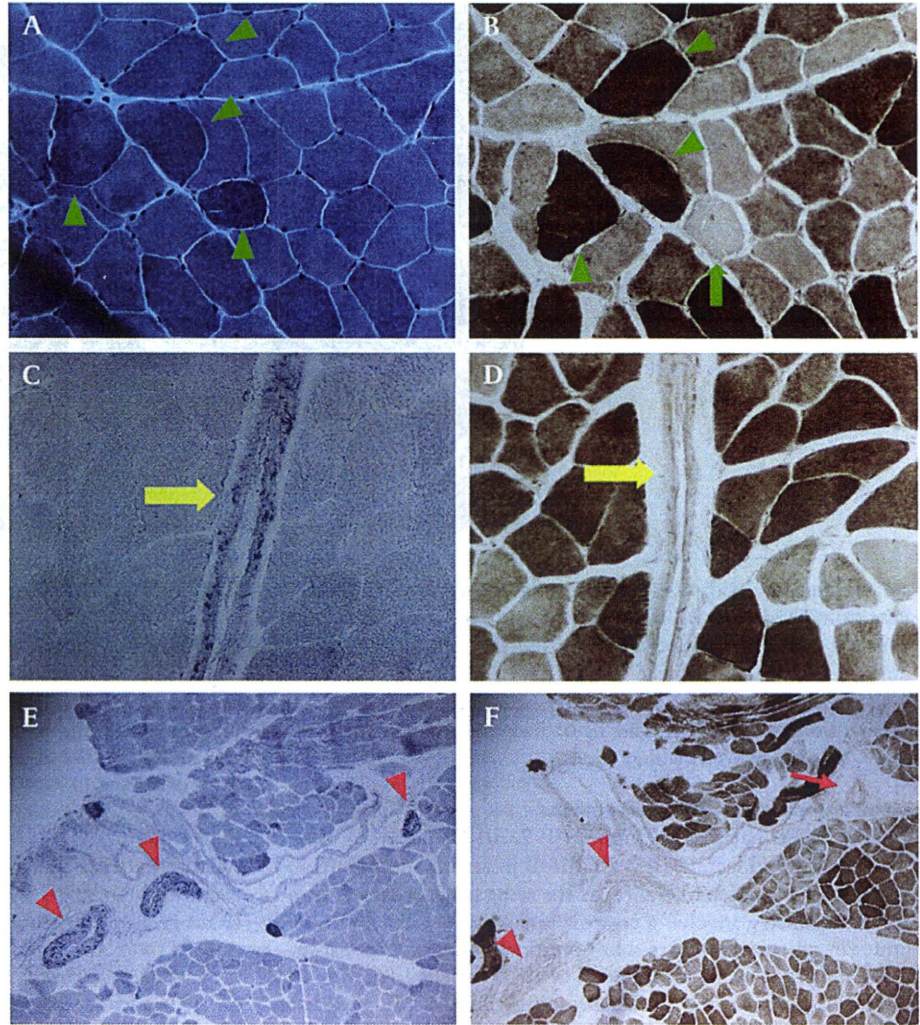


Figure 1 Proband's family pedigree. ○ = woman; □ = man; / = deceased. Solid symbols are symptomatic members. The arrow shows the proband. * Patients we encountered.

Figure 2 Pathology observed in *rectus femoris* muscle biopsies in III-1 (A and B) and II-2 (C, D, E and F). A and B, C and D, and E and F are pairs of adjacent sections stained as indicated. (A) Scattered ragged-red fibers (RRFs). Modified Gomori trichrome stain, $\times 400$. (B) Occasional RRFs with (arrowheads) or without (arrow) cytochrome c oxidase (COX) activities. COX stain, $\times 400$. (C) Strongly succinate dehydrogenase-reactive blood vessels (SSVs) (arrow). Succinate dehydrogenase (SDH) stain, $\times 400$. D; SSVs with COX activities (arrow). COX stain, $\times 400$. (E) SSVs (arrowheads). SDH stain, $\times 100$. (F) SSVs without COX activities (arrowheads) and with mild COX activities (arrow). COX stain, $\times 100$.



or additions of, other antiepileptic drugs (phenytoin, zonisamide, topiramate, sodium valproate), control of seizures was difficult, and she required intensive care with mechanical ventilation twice during status epilepticus (SE). Moreover, in the course of treatment for the second SE, abdominal pain and elevated serum amylase and lipase occurred. A CT scan and an ultrasonogram detected no abnormal changes in the pancreas. Following treatment with camostat mesilate, ursodeoxycholic acid and ulinastatin, the symptoms were relieved and serum pancreatic enzymes were normalised in 1 month.

II-1: mother of III-1

The proband's mother, at age 51, was asymptomatic.

mtDNA mutation analysis

The examination of mtDNA mutations was first conducted in II-2 at another institution. She appeared to express the features of both MERRF and MELAS. Therefore, two established pathogenic mutations in mtDNA found in these phenotypes, m.8356T>C and m.3243G>A, were selected and screened for using commercial-based analyses of blood (SRL Inc.); both point mutations were found. Therefore, we also screened for these mtDNA mutations in blood and muscle of III-1 and in the preserved muscle specimen of II-2. The m.8356T>C and m.3243A>G mutations were detected by PCR-restriction frag-

ment length polymorphism analysis. Genomic DNA was extracted from blood and muscle specimens and amplified by PCR. PCR primers for m.3243A>G were adopted from Goto *et al.*⁸ while mismatch primers to detect m.8356T>C substitution were adopted from Silvesti *et al.*⁴ PCR products were digested with *Apa*I and *Dra*I at positions 3243 and 8356, respectively. Plasmids containing only wild-type or mutant mtDNA were constructed and used as controls. PCR products were also sequenced to confirm the base substitutions. Blood samples of two other family members whom we had chances to examine (II-1 and III-6) were also analysed with the same procedure. Moreover, whole mtDNA genome analyses in blood and muscle of III-1 and in blood of II-1 were conducted (mito-SEQr resequencing system, for resequencing the entire mitochondrial genome with 46 RSAs. Applied Biosystems, USA).

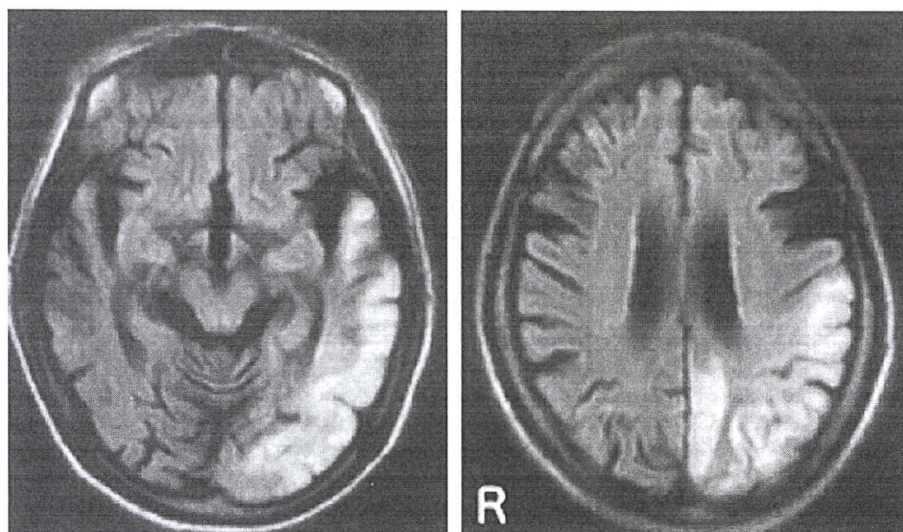
RESULTS

Symptoms and phenotypes

The phenotypes of the proband (III-1) and cousin (III-6) were MERRF, the aunt (II-2) was MERRF/MELAS overlap syndrome and the mother (II-1) was an asymptomatic carrier. Three other members (I-1, III-5 and III-7) also had some symptoms that could not be categorised in distinct entities. Of the three patients with MERRF (III-1 and III-6) and MERRF/MELAS overlap syndrome (II-2), two (II-2 and III-1) showed short

Original article

Figure 3 Brain MRI of II-2 during acute phase. FLAIR images detected a hyperintense lesion extending from the left occipito-parieto-temporal lobe at 38 years. R: right.



stature and low body weight with bilateral sensorineural deafness from childhood. All three patients suffered from myoclonic epilepsy from the late teens to the mid-20s. Patient II-2 subsequently exhibited episodic headache in her mid-30s, with a stroke-like episode that repeatedly occurred afterwards. The other two patients (III-1 and III-6) had not reached their 30s when this study was conducted.

Blood and cerebrospinal fluid analysis

Of the three patients examined (II-2, III-1 and III-6), two showed elevated lactate (II-2 and III-6) in serum and one (II-2) had impaired glucose tolerance; at the same time, other items in serum chemistry, involving creatine kinase, were within normal limits in all three patients. No hormonal abnormalities except short stature were found in blood of III-1. Patient III-1 showed high levels of lactate in cerebrospinal fluid (CSF was not examined in the other patients).

Radiological examinations and EEG findings

Of the three patients examined, brain MRIs in two of them (II-2 and III-1) showed diffuse brain atrophy, with stroke-like lesions in II-2, while patient III-6 exhibited a normal brain MRI. Transthoracic ultrasonic cardiographies demonstrated normal cardiac wall motion in the two patients examined (III-1 and III-6). Thoracic and abdominal CT scans detected no abnormalities in III-1. Two patients (III-1 and III-6) underwent EEG. III-1 showed generalised slow waves, and III-6 exhibited focal spike-and-waves.

Muscle pathology

Muscle biopsies were conducted in two cases (II-2 and III-1). II-2 had already expressed stroke-like episodes at the time this procedure was conducted. The two patients had similar morphological findings: fibre size variability, RRFs, focal COX deficiency, SSVs and a mosaic distribution of COX activities in both RRFs and SSVs (figure 2). The proportion of the SSVs with COX deficiencies was higher in III-1 than in II-2.

Genetic analysis

Results of genetic analyses are shown in figure 4. Genetic analysis of mtDNA in III-1 revealed heteroplasmic m.8356T>C and m.3243A>G mutations in blood. This double mtDNA mutation was also detected and was heteroplasmic in the blood of II-1 and

III-6, although the proportions of both mutations were clearly less in asymptomatic II-1. In muscle of III-1, the proportion of m.3243A>G was higher than that in blood and m.8356T>C appeared to be homoplasmic. In muscle of II-2, m.3243A>G was heteroplasmic and m.8356T>C also appeared to be homoplasmic. Screening of the entire mtDNA genomes from blood and muscle of III-1 and from blood of II-1 revealed no mutations other than the m.8356T>C and m.3243G>A transitions.

Discussion

All four patients that we encountered carried the double-point mutations m.8356T>C and m.3243A>G in mitochondrial tRNA genes. Both mutations were heteroplasmic in blood, while m.8356T>C appeared to be homoplasmic in muscle. The proportion of m.3243A>G transitions was higher in the muscle of III-1 and seemed to be associated with clinical severity because all symptomatic patients had significant proportions of the mutation, but the asymptomatic patient II-1 carried the lowest mutational load. The m.8356T>C mutation appeared to be homoplasmic in muscle of III-1 and II-2, although a low level

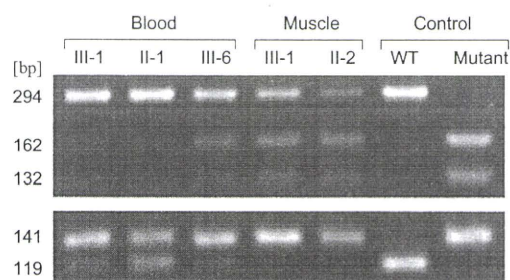


Figure 4 Restriction fragment length polymorphism analysis for the m.3243A>G and m.8356T>C mutations. Upper panel demonstrates variable heteroplasmy level of the m.3243A>G mutation in the pedigree. Uncut 294 bp band represents the wild type (3243A) while the 162 and 132 bp bands represent the mutant (3243G). Ratio of the mutant in muscle is significantly higher than in blood of III-1. Lower panel also shows variable heteroplasmy level of the m.8356T>C mutation. Uncut 141 bp band represents the mutant (8356C) while the 119 and 22 bp bands (only the 119 bp band is shown) represent the wild-type (8356T). The mutation rate in muscle is higher than in blood and appears to be homoplasmic in III-1 and II-2. WT and Mutant represent cloned plasmid DNAs containing only wild-type and mutation sequences, respectively.

of heteroplasmy cannot be excluded due to the limitation of our current semi-quantitative PCR analysis. Nevertheless, it is fair to say that the m.8356T>C transition was higher in muscle than in blood, at least in III-1. The proportion of m.8356T>C transitions also appeared to be associated with clinical severity.

The four patients showed phenotypes of MERRF (III-1 and III-6), MERRF/MELAS overlap syndrome (II-2) and of an asymptomatic carrier (II-1). There were several other symptomatic family members (I-1, III-5 and III-7). We suggest that the typical course of disease in this family is as follows: the onset is characterised by short stature with emaciation and bilateral sensorineural deafness in childhood followed by cerebellar ataxia and myoclonic epilepsy; MERRF expression follows in young adulthood. By middle age, the disease progression is characterised by the addition of migraine, vomiting and stroke-like episodes, symptoms of MELAS expression that indicate completion of the MERRF/MELAS overlap syndrome. Muscle pathology is compatible with MELAS before and after phenotypic expression of MELAS.^{9 23} However, a quantitative association between SSVs with COX deficiencies and expression of MELAS was not found in this study. This might mean that these family members gain the potential to express MELAS from the mutation loads in their primary phases. The characteristic brain MRI and EEG findings were not observed in this family. Neither were external ophthalmoplegia nor cardiomyopathy detected.

We presume that these mutations are pathogenic for the observed clinical phenotypes based on the following criteria; (1) m.8356T>C and m.3243A>G transitions are pathogenic for MERRF^{5 6} and MELAS,⁸ respectively; (2) both mutations were heteroplasmic in blood of all four cases; (3) no mutations other than m.8356T>C and m.3243A>G were detected in total sequences of mtDNA from blood of II-1 or from blood and muscle of III-1; (4) other symptomatic members of the pedigree had symptoms indicative of mitochondrial dysfunction.²

Patients with the m.8356T>C transition frequently express both MERRF and MELAS.^{5 6} Moreover, some patients with the m.3243A>G transition exhibit MERRF^{10 11} or MERRF/MELAS overlap syndrome.^{12 13} As we did not quantitatively evaluate these mutations or clarify their thresholds, we were unable to determine whether both mutations simultaneously affected the observed clinical phenotypes.

In II-2, with MERRF/MELAS overlap syndrome, MERRF preceded MELAS. In the next generation, the proband (III-1) expressed MERRF without MELAS. However, her muscle pathology showed RRFs and SSVs with COX activities, which are more characteristic of MELAS than MERRF,²³ and SSVs might be a predictor of stroke-like episodes²⁴ and additional MELAS expression. This finding leads us to speculate that the m.3243A>G transition might be pathogenic for expressing MELAS. Because the proportion of another mtDNA point mutation in muscle (m.12320A>G) was shown to increase overtime,²⁵ we hypothesise that the possibly increasing m.8356T>C transitions in our family might first overcome the threshold for the biochemical and symptomatic expressions of MERRF, and the increasing m.3243A>G transitions might then finally reach the threshold of symptomatic MELAS expression. It is presumed that neither mutation had reached its threshold in the asymptomatic family members. However, to demonstrate the pathogenicity of the m.3243A>G transition in the expression of MELAS, single-muscle fibre studies and more precise mtDNA species analyses are required. Without these data, it remains unknown whether a stroke-like episode of patient II-2 may be ascribed to m.3243A>G, because the m.8356T>C mutation itself can lead to the expression of MELAS/MERRF

overlap syndrome.^{5 6} Among further studies that we are planning, the screening for m.3243A>G transitions in urinary sediment samples will also be informative for determining clinical severity. Data have shown that assessment of mtDNA mutational load in urinary cells correlates closely with that observed in skeletal muscle^{26 27} and is also a reliable measure of clinical severity.²⁸

Most of the reported cases of patients with more than one mtDNA mutation carried double-point mutations^{15–22}, however, cases with two heteroplasmic mtDNA point mutations were observed by Bidooki *et al* in only one family with m.10010T>C and m.5656A>G transitions in the tRNA^{Gly} gene and in the non-coding region between the tRNA^{Asn} and tRNA^{Aln} genes, respectively.¹⁶ The former mutation was pathogenic, while the latter was silent, and the associated phenotypes have not been generally established even in the former.¹⁶ By contrast, both of the mutations in our family are known to express established phenotypes. The difference between this work and the 1997 publication by Bidooki *et al*¹⁶ is that in the current study, there are potentially two pathogenic mtDNA mutations rather than a pathogenic mutation and a SNP. However, the causal effects must be investigated experimentally.

There are, as yet, no reports of double mtDNA mutations in which no evolutionary associations with one another were shown.^{15–22} Thus, we presume that some of the double mutations in our family were in the same mitochondria and some occurred as single mutations in distinct mitochondria. If further studies demonstrate this condition (ie, the recombination of mtDNA¹⁶ and one mutation's effect arising along with another in mtDNA²⁹), single muscle fibre analysis and quantitative evaluations of the heteroplasmic rate of both mutations in each tissue might provide more profound insights into mtDNA mutations.

Main messages

- ▶ This is the first reported case of a double point mutation (m.8356T>C and m.3243A>G) in mitochondrial DNA (mtDNA), both of which were heteroplasmic and pathogenic for the mitochondrial encephalomyopathy phenotypes of myoclonic epilepsy with ragged-red fibers (MERRF) and mitochondrial encephalopathy, lactic acidosis, and stroke-like episodes (MELAS).
- ▶ Phenotypes of the four patients in this family were MERRF, MERRF/MELAS overlap syndrome, and asymptomatic carrier.
- ▶ All four patients carried double point mutations, m.8356T>C and m.3243A>G transitions, in mitochondrial tRNA genes. Both mutations were heteroplasmic in blood, while m.8356T>C appeared to be homoplasmic in muscle.

Current research questions

- ▶ Further studies will demonstrate this condition (ie, the recombination of mtDNA and one mutation's effect arising along with another in mtDNA). Single muscle fiber analysis and quantitative evaluations of the heteroplasmic rate of both mutations in each tissue might provide more profound insights into mtDNA mutations.

Original article

Acknowledgements We thank all patients for their active cooperation. This work was supported in part by a Grant-in-Aid for Scientific Research from the Ministry of Education, Science, Sports and Culture, Japan and by a grant from the Uehara Foundation.

Competing interests None.

Patient consent Obtained.

Ethics approval This study was conducted with the approval of the Hokkaido University Ethics Committee.

Provenance and peer review Not commissioned; externally peer reviewed.

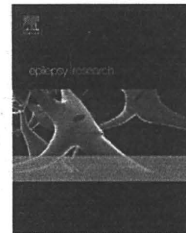
REFERENCES

1. Fukuhara N, Tokiguchi S, Shirakawa K, Tsubaki T. Myoclonus epilepsy associated with ragged-red fibers (mitochondrial abnormalities): disease entity or a syndrome? *J Neurol Sci* 1980;**47**:117–33.
2. DiMauro S, Moraes CT. Mitochondrial encephalomyopathies. *Arch Neurol* 1993;**50**:1197–208.
3. Shoffner JM, Lott MT, Lezza AM, Seibel P, Ballinger SW, Wallace DC. Myoclonic epilepsy and ragged-red fibers (MERRF) is associated with a mitochondrial DNA tRNA^{Leu} mutation. *Cell* 1990;**61**:931–7.
4. Silvestri G, Moraes CT, Shanske S, Oh SJ, DiMauro S. A new mtDNA mutation in the RNA^{Leu} gene associated with myoclonus epilepsy and ragged-red fibers (MERRF). *Am J Hum Genet* 1992;**51**:1213–7.
5. Sano M, Ozawa M, Shiota S, Momose Y, Uchigata M, Goto Y. The T-C⁽⁸³⁵⁶⁾ mitochondrial DNA mutation in a Japanese family. *J Neurol* 1996;**243**:441–4.
6. Zeviani M, Muntoni F, Savarese N, Serra G, Tiranti V, Carrara F, Mariotti C, DiDonato S. A MERRF/MELAS overlap syndrome associated with a new point mutation in the mitochondrial DNA tRNA^{Leu} gene. *Eur J Hum Genet* 1993;**1**:80–7.
7. Pavlakis SG, Phillips PC, DiMauro S, De Vivo DC, Rowland LP. Mitochondrial myopathy, encephalopathy, lactic acidosis, and stroke like episodes: a distinctive clinical syndrome. *Ann Neurol* 1984;**16**:481–8.
8. Goto Y, Nonaka I, Horai S. A mutation in the tRNA^{Leu(UUR)} gene associated with the MELAS subgroup of mitochondrial encephalomyopathies. *Nature* 1990;**348**:651–3.
9. Goto Y. Clinical features of MELAS and mitochondrial DNA mutations. *Muscle Nerve* 1995;**3**:107–12.
10. Folgero T, Torbergesen T, Oian P. The 3243 MELAS mutation in a pedigree with MERRF. *Eur Neurol* 1995;**35**:168–71.
11. Fabrizi GM, Cardaioli E, Grieco GS, Cavallaro T, Malandrini A, Manneschi L, Dotti MT, Federico A, Guazzi G. The A to G transition at nt 3243 of the mitochondrial (RNA^{Leu(UUR)}) may cause a MERRF syndrome. *J Neurol Neurosurg Psychiatr* 1996;**61**:47–51.
12. Campos Y, Martin MA, Lorenzo G, Aparicio M, Cabello A, Arenas J. Sporadic MERRF/MELAS associated with the 3243 tRNA^{Leu(UUR)} mutation of mitochondrial DNA. *Muscle Nerve* 1996;**19**:187–90.
13. Mongini T, Doriguzzi C, Chiadò-Piat L, Silvestri G, Servidei S, Palmucci L. MERRF/MELAS overlap syndrome in a family with A3243G mtDNA mutation. *Clin Neuropathol* 2002;**21**:72–6.
14. Verma A, Moraes CT, Shebert RT, Bradley WG. A MERRF/PEO overlap syndrome associated with the mitochondrial DNA 3243 mutation. *Neurology* 1996;**46**:1334–6.
15. Riordan-Eva P, Sanders MD, Govan GG, Sweeney MG, Da Costa J, Harding AE. The clinical features of Leber's hereditary optic neuropathy defined by the presence of a pathogenic mitochondrial DNA mutation. *Brain* 1995;**118**:319–37.
16. Bidooki SK, Johnson MA, Chrzanowska-Lightowlers Z, Bindoff LA, Lightowlers RN. Intracellular mitochondrial triplasm in a patient with two heteroplasmic base changes. *Am J Hum Genet* 1997;**60**:1430–8.
17. Arenas J, Campos Y, Bornstein B, Ribacoba R, Martín MA, Rubio JC, Santorelli FM, Zeviani M, DiMauro S, Garesse R. A double mutation (A8296G and G8363A) in the mitochondrial DNA tRNA^{Leu} gene associated with myoclonus epilepsy with ragged-red fibers. *Neurology* 1999;**52**:377–82.
18. Brown MD, Allen JC, Van Stavern GP, Newman NJ, Wallace DC. Clinical, genetic, and biochemical characterization of a Leber hereditary optic neuropathy family containing both the 11778 and 14484 primary mutations. *Am J Med Genet* 2001;**104**:331–8.
19. Mimaki M, Ikota A, Sato A, Komaki H, Akanuma J, Nonaka I, Goto Y. A double mutation (G11778A and G12192A) in mitochondrial DNA associated with Leber's hereditary optic neuropathy and cardiomyopathy. *J Hum Genet* 2003;**48**:47–50.
20. Tonska K, Kurzawa M, Ambroziak AM, Korwin-Rujna M, Szaflik JP, Grabowska E, Szaflik J, Bartnik E. A family with 3460G>A and 11778G>A mutations and haplogroup analysis of Polish Leber hereditary optic neuropathy patients. *Mitochondrion* 2008;**8**:383–8.
21. Dai D, Lu Y, Chen Z, Wei Q, Cao X, Xing G. Co-segregation of the T1095C with the A1555G mutation of the mitochondrial 12S rRNA gene in a patient with non-syndromic hearing loss. *Biochem Biophys Res Commun* 2008;**377**:1152–5.
22. Zhang AM, Jia X, Yao YG, Zhang Q. Co-occurrence of A1555G and G11778A in a Chinese family with high penetrance of Leber's hereditary optic neuropathy. *Biochem Biophys Res Commun* 2008;**376**:221–4.
23. Goto Y, Horai S, Matsuoka T, Koga Y, Nihei K, Kobayashi M, Nonaka I. Mitochondrial myopathy, lactic acidosis, and stroke-like episodes (MELAS): a correlative study of the clinical features and mitochondrial DNA mutation. *Neurology* 1992;**42**:545–50.
24. Hasegawa H, Matsuoka T, Goto Y, Nonaka I. Strongly succinate dehydrogenase-reactive blood vessels in muscles from patients with mitochondrial myopathy, encephalopathy, lactic acidosis, and stroke-like episodes. *Ann Neurol* 1991;**29**:601–5.
25. Weber K, Wilson JN, Taylor L, Brierley E, Johnson MA, Turnbull DM, Bindoff LA. A new mtDNA mutation showing accumulation with time and restriction to skeletal muscle. *Am J Hum Genet* 1997;**60**:373–80.
26. McDonnell MT, Schaefer AM, Blakely EL, McFarland R, Chinnery PF, Turnbull DM, Taylor RW. Noninvasive diagnosis of the 3243A>G mitochondrial DNA mutation using urinary epithelial cells. *Eur J Hum Genet* 2004;**12**:778–81.
27. Shanks S, Pancrudo J, Kaufmann P, Engelstad K, Jung S, Lu J, Naini A, DiMauro S, De Vivo DC. Varying loads of the mitochondrial DNA A3243G mutation in different tissues: implications for diagnosis. *Am J Med Genet A* 2004;**130**:134–7.
28. Whittaker RG, Blackwood JK, Alston CL, Blakely EL, Elson JL, McFarland R, Chinnery PF, Turnbull DM, Taylor RW. Urine heteroplasmy is the best predictor of clinical outcome in the m.3243A>G mtDNA mutation. *Neurology* 2009;**72**:568–9.
29. Ohno K, Yamamoto M, Engel AG, Harper CM, Roberts LR, Tan GH, Fatourechhi V. MELAS and Kerns-Sayre-type communication with myopathy and autoimmune polyendocrinopathy. *Ann Neurol* 1996;**39**:761–6.



ELSEVIER

journal homepage: www.elsevier.com/locate/epilepsyres



The applications of time-frequency analyses to ictal magnetoencephalography in neocortical epilepsy

Kazuyori Yagyu^{a,*}, Fumiya Takeuchi^b, Hideaki Shiraishi^a, Shingo Nakane^c, Keitaro Sueda^a, Naoko Asahina^a, Shinobu Kohsaka^a, Shuichi Umeoka^d, Naotaka Usui^d, Koichi Baba^d, Shinji Saitoh^a

^a Department of Pediatrics, Hokkaido University Graduate School of Medicine, Japan

^b Faculty of Health Sciences, Hokkaido University Graduate School of Health Sciences, Japan

^c Division of Magnetoencephalography, Hokkaido University Hospital, Japan

^d Department of Neurosurgery, National Epilepsy Center, Shizuoka Institute of Epilepsy and Neurological Disorders, Japan

Received 14 June 2009; received in revised form 13 January 2010; accepted 2 May 2010

Available online 1 June 2010

KEYWORDS

Ictal onset;
Propagation;
Polyspike;
Short-time Fourier transform;
Ictal discharge;
Rhythmic activities

Summary

Purpose: Ictal magnetoencephalographic (MEG) discharges convey significant information about ictal onset and propagation, but there is no established method for analyzing ictal MEG. This study sought to clarify the usefulness of time-frequency analyses using short-time Fourier transform (STFT) for ictal onset and propagation of ictal MEG activity in patients with neocortical epilepsy.

Methods: Four ictal MEG discharges in two patients with perirolandic epilepsy and one with frontal lobe epilepsy (FLE) were evaluated by time-frequency analyses using STFT. Prominent oscillation bands were collected manually and the magnitudes of those specific bands were superimposed on individual 3D-magnetic resonance images.

Results: STFT showed specific rhythmic activities from alpha to beta bands at the magnetological onset in all four ictal MEG records. Those activities were located at the vicinity of interictal spike sources, as estimated by the single dipole method (SDM), and two of the four ictal rhythmic activities promptly propagated to ipsilateral or bilateral cerebral cortices. The patients with FLE and perirolandic epilepsy underwent frontal lobectomy and resection of primary motor area, respectively including the origin of high-magnitude areas of a specific band indicated by STFT, and have been seizure free after the surgery.

* Corresponding author at: Department of Pediatrics, Hokkaido University Graduate School of Medicine, North 15, West 7, Kita-ku, Sapporo, Hokkaido 060-8638, Japan. Tel.: +81 11 706 5954; fax: +81 11 706 7898.

E-mail address: kazuyori@med.hokudai.ac.jp (K. Yagyu).



Conclusions: STFT for ictal MEG discharges readily demonstrated the ictal onset and propagation. These data were important for decisions on surgical procedure and extent of resection. Ictal MEG analyses using STFT could provide a powerful tool for noninvasive evaluation of ictal onset zone.

© 2010 Elsevier B.V. All rights reserved.

Introduction

Precise localization of ictal onset and propagation in patients with symptomatic localization-related epilepsy (SLRE) is critical, especially in candidates for epilepsy surgery. Magnetoencephalography (MEG) is a new tool for assessing epileptic current that shows superior spatial and temporal resolution over the standard EEG (Hämäläinen et al., 1993). The single dipole method (SDM) is a useful way to monitor interictal MEG epileptiform activity (Stefan et al., 2003), although a method for analyzing MEG-measured ictal activity has not been established.

The ictal onset area was successfully demonstrated in cases with *epilepsia partialis continua* using a combination of jerk-locked back averaging and SDM with MEG (Shigeto et al., 1997; Oishi et al., 2002a). Tilz et al. (2002) also analyzed ictal MEG activities by SDM for epileptic patients that predominantly experienced mesial temporal lobe epilepsy. This study determined the ictal onset area successfully in 6 out of 13 cases, while SDM was not available in the remaining patients. In another study of MEG analyses for ictal rhythmic activities in four cases with medial frontal lobe epilepsy (FLE), SDM was not applicable for two of these cases, while one case had no significant spike at the onset zone in ictal MEG discharges, and the remaining patient showed no reliable spike sources by SDM (Shiraishi et al., 2001). The latter two cases were considered inapplicable for the SDM formula because the signals had already propagated broadly. Jongh et al. (2003) concluded that in patients with SLRE and brain tumor, interictal fast activities of 8–50 Hz did not localize to the tumor borders, and that SDM was not useful for analyzing fast waves in such cases.

SDM is an established procedure for analyzing single or spatially and temporally limited activities such as interictal epileptiform activities; however, it has limitations for analyzing spatially propagated and temporally prolonged rhythmic magnetological activity including ictal data during the secondary generalization. Nevertheless, ictal activities contain valuable information (Tilz et al., 2002; Jongh et al., 2003), and a reliable confirmatory method for analyzing ictal MEG is needed.

Rhythmic ictal discharge of EEG in SLRE reflects the precise location of ictal onset (Westmoreland, 1998; Verma and Radtke, 2006). Furthermore, Guggisberg et al. (2008) recently reported that fast oscillations associated with interictal spikes in MEG detected by spike-locked frequency analysis successfully demonstrated the localized epileptogenic zone.

The present study analyzed the localization of ictal rhythmic activity onset and propagation using time-frequency analysis by short-time Fourier transform (STFT) in patients with neocortical epilepsy. The locations of specific-frequency bands were also correlated with conventional SDM results for interictal epileptiform spikes sources and with prognosis following surgical treatment.

Patients and methods

Patients

Case 1. A 12-year-old girl with FLE. She had a past history of neonatal left-middle cerebral artery infarction. Seizures started at the age of 3 years presented as atonic seizure on the right side of her body, and postural seizure with right-limb extension. Her seizures occurred daily even with multiple antiepileptic drugs (AEDs). Brain MRI revealed an encephalomalacia at the left-frontal and parietal lobes (Fig. 1A, left).

Case 2. A 14-year-old boy with perirolandic epilepsy. His seizures started at the age of 8 years, beginning with somatosensory auras (tingling in the right hand) and evolving into right hemiconvulsion with his face and eyes deviated to the right side. His seizures were precipitated by touch on the right side of his body and occurred daily even with multiple AEDs. Brain MRI demonstrated no abnormality. [18F]-fluorodeoxyglucose positron emission tomography (FDG-PET) showed glucose hypometabolism at the left postcentral gyrus (Fig. 2A).

Case 3. A 25-year-old woman with perirolandic epilepsy. Her seizures started at the age of 10 years, beginning with somatosensory auras in the left ear and evolving into complex partial seizures. The seizures were always precipitated by touch on the left side of her body and occurred daily in spite of multiple AEDs. She had no brain lesion on MRI or [18F]-FDG-PET.

In all cases, guardians gave written informed consent for this study.

MEG data analyses

MEG data were recorded using a 204-channel, helmet-shaped gradiometer (Vectorview System, Elekta-Neuromag Oy, Stockholm, Sweden) from patients in a supine position in a magnetically shielded room, and collected for about 40 min from each patient using a 600-Hz sampling rate. During the MEG recording, scalp EEGs were also recorded simultaneously using the international 10–20 system.

The segments containing ictal and interictal paroxysms were selected manually. The raw MEG data were filtered with band-pass filtering of 0.03–133 Hz for offline analyses. We used SDM for localized interictal epileptiform activities and STFT for ictal rhythmic polyspike epileptiform discharges to determine the onset and propagation of the ictal discharges.

Single dipole method (SDM)

Dipole-fit software (Neuromag Oy, Helsinki, Finland) was used to calculate the equivalent current dipoles (ECDs). We defined acceptable ECDs by a goodness of fit (GOF) higher than 70%; this value measures how well the ECD model explains the measured signals. Acceptable ECDs were superimposed on the individual MRIs.

Short-time Fourier transform (STFT) analyses

STFT was used to show the distribution of MEG polyspikes (Oppenheim and Schaffer, 1999) and the MATLAB (MathWorks, Natick, MA, USA) program was used to apply STFT to the MEG signals. Each signal was divided into defined sequential frames, and fast Fourier transformation (FFT) was applied to each frame.

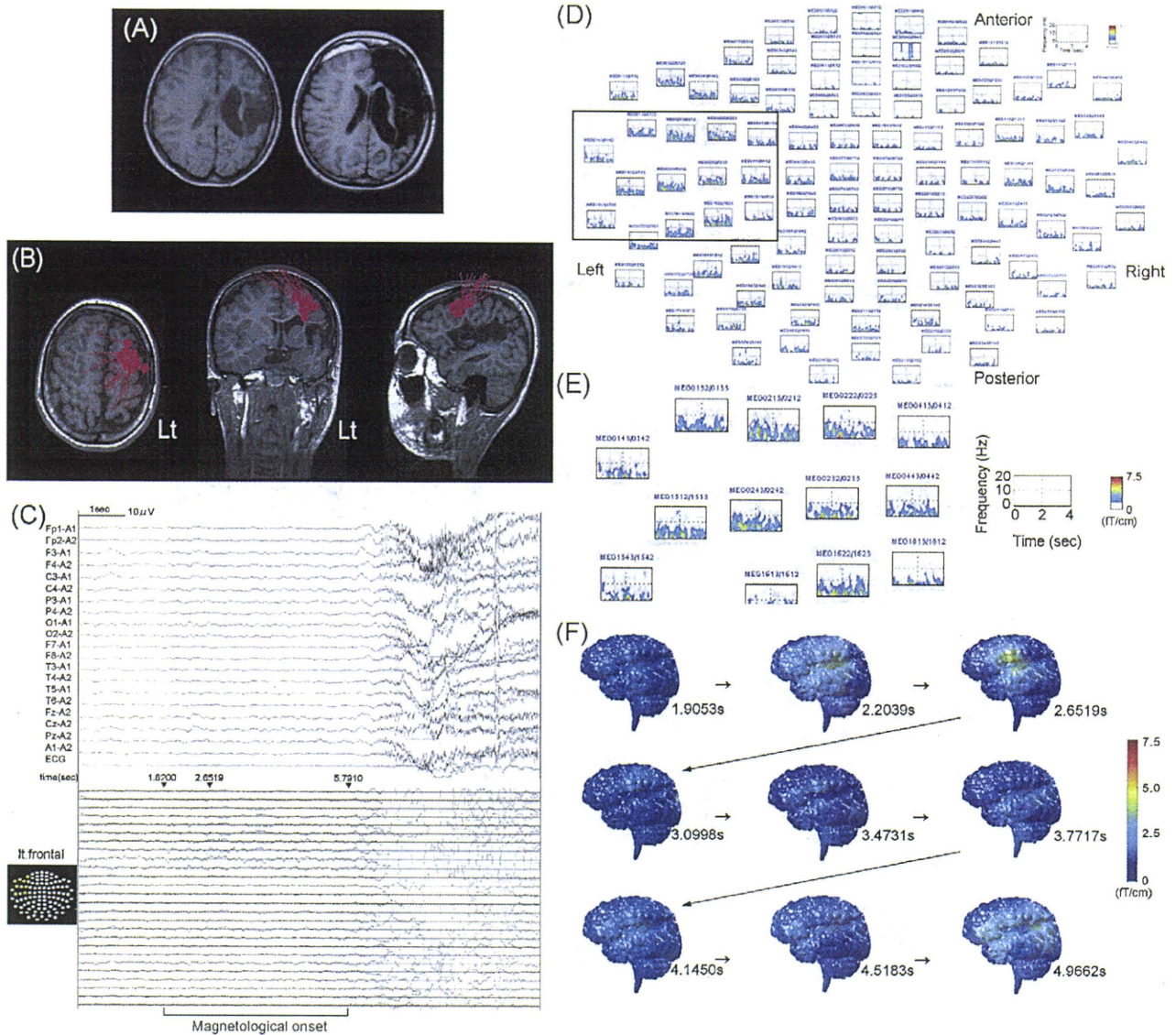


Figure 1 (A) Case 1 MRI: MRI before (left) and after (right) the operation showed encephalomalacia in the left hemisphere (left) and an operation scar in the left-frontal lobe (right). (B) Case 1 SDM: Interictal spike sources were estimated to lie near the posterior lateral area of the left-frontal lobe (red dot). (C) Case 1 ictal EEG and MEG: representative ictal EEG (top) showing a left-frontal slow wave followed by left-frontal dominant polyspikes; MEG at the left-frontal area (bottom) showing rhythmic discharges with a 7–20-Hz band oscillation (magnetological onset). (D) Case 1 MEG/STFT: analysis of graph by STFT for magnetological onset duration of (C) (4.0s), showing up to 12-Hz oscillations at the left-frontal area. (E) Case 1 MEG/STFT: representative STFT illustration of MEG channel at the left-frontal area (corresponding to the boxed area of (D)) showing specific oscillations of up to 12 Hz (yellow and red areas). (F) Case 1 3D-MRI overlay: sequential demonstration of specific-frequency band magnitudes projected on 3D-MRIs. Color bar indicates the magnitude of a specific-frequency band and numbers on the right lower part demonstrate the time scale corresponding to (C). (For interpretation of the references to color in this figure legend, the reader is referred to the web version of the article.)

In the present study, STFT was implemented using a 256-point window. The time of each window was 426.7 ms (i.e., 256 points \times 1000 ms/600 Hz), and the window was shifted every four points, which corresponded to 6.7 ms (i.e., 1000 ms/600 Hz \times 4 points). FFT applied to each window. This process was repeated for all selected signals. The time-frequency distributions are displayed graphically.

Selection of specific-frequency bands and projection to 3D-MRIs

The time-frequency distributions were analyzed up to 133 Hz and for 10s until ictal motion artifact started. Specific-frequency bands that appeared continuously and were prominent from background activities were selected man-

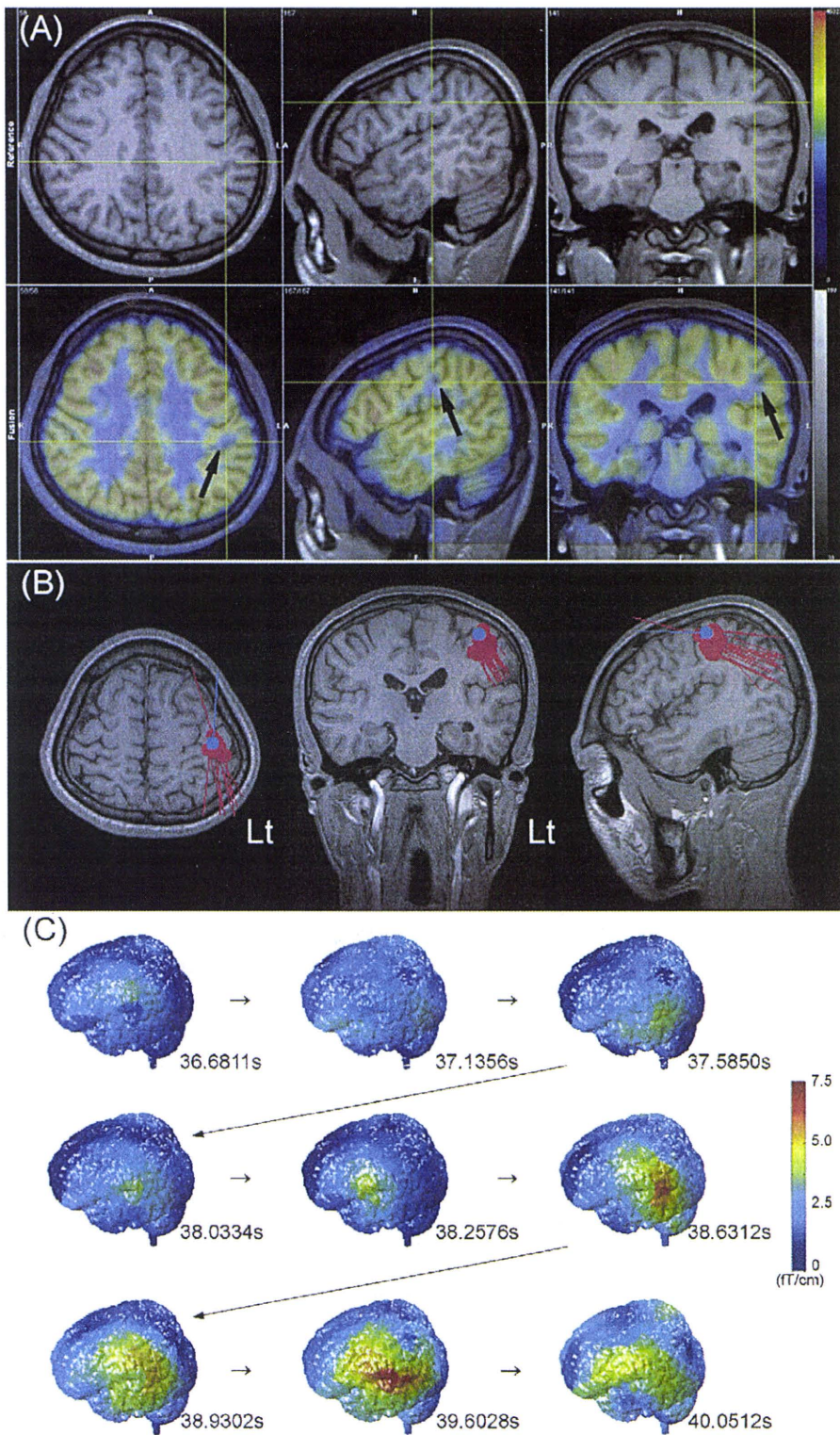


Figure 2 (A) Case 2 [18F]-FDG-PET: MRI (top) and [18F]-FDG-PET (bottom) showing hypometabolism of glucose consumption at the left postcentral gyrus (arrow). (B) Case 2 SDM: blue dot indicates somatosensory-evoked field and red dots indicate spike sources estimated by SDM. Those spike sources were estimated in the left postcentral gyrus. (C) Case 2 3D-MRI overlay: high-magnitude zone of 10–15 Hz oscillation was generated from the left parietal and temporal lobes and followed by propagation to the bilateral temporal and parietal lobes. Color mapping of 3D-MRI indicates the magnitudes of specific-frequency bands (10–15 Hz). (For interpretation of the references to color in this figure legend, the reader is referred to the web version of the article.)

ually. Thus, the duration of graphs and selected bands varied.

The specific-frequency bands selected were then projected to individual 3D-MRIs. The power spectrum of these bands on 3D-MRI was located at the intersection of the line beneath the planer gradiometer coil and brain surface.

Electrocorticography (ECoG)

To define the epileptogenic focus, chronic subdural electrodes were implanted to analyze the location of ictogenesis, according to the interictal and ictal scalp EEG and MEG results. Electrocorticography (ECoG) was conducted using Neurofax-1000 (Nihon-Kohden, Tokyo, Japan) amplifiers at a sampling rate of 1 kHz and time constant at 10 s with grid platinum/iridium electrodes (2.3-mm diameter, 10-mm inter-electrode spacing, Ad-Tech, Racine, WI). High frequent oscillation (HFO) was analyzed by ECoG, with 53–300 Hz band-pass filtering.

Results

Case 1

The interictal EEG showed left-frontal dominant polyspikes, polyspikes and wave complex. SDM analysis of the MEG showed clustered spike sources at the left-frontal lobe in the vicinity of the encephalomalacia (Fig. 1B). Ictal EEG showed left-frontal slow waves followed by left-frontal dominant polyspikes (Fig. 1C, top).

Ictal MEG data with 4.0 s prior to ictal motion artifact analyzed by STFT (Fig. 1C, bottom) showed left-frontal dominant rhythmic magnetological activities of 7–12 Hz (Fig. 1D and E). These high-magnitude areas of activity were located at the left superior-frontal gyrus on 3D-MRI (Fig. 1F), which was consistent with the spike sources estimated by SDM (Fig. 1B). We also applied SDM to the ictal MEG data; however, ECDs were scattered broadly over the left-frontal to occipital lobe regions and GOF was generally very low (<50%). Based on the STFT results and other noninvasive examinations, we predicted the ictal onset zone location as anterior to the ischemic scar.

After noninvasive presurgical evaluation, the patient underwent long-term intracranial EEG monitoring with subdural electrodes. Electrical stimulation in the vicinity of the left premotor area induced the patient's habitual seizure. The ictal ECoG were captured once and a low-amplitude HFO of 200–300 Hz was detected at the superior-frontal gyrus in pre-ictal period. She underwent frontal lobectomy including the high-magnitude areas of the ictal MEG (Fig. 1A, right). She has been seizure free for a year since surgery and has no mental or motor deficit.

Case 2

This patient showed left central and parietal spikes interictally by EEG. SDM analysis of the interictal MEG showed clustered spike sources at the left postcentral gyrus (Fig. 2B).

Ictal EEG demonstrated diffuse 10-Hz polyspikes bilaterally. Analysis of the ictal MEG data with 4.0 s duration prior to ictal motion artifact by STFT showed specific rhythmic activities of 10–15 Hz at the magnetological onset of the seizure. Those ictal activities originated from the left pari-

etal and temporal lobes, and propagated to the bilateral parietal and temporal lobes (Fig. 2C). The ictal onset zone defined by ictal MEG was in the vicinity of interictal spike sources estimated by SDM. This result was consistent also with the localization of glucose hypometabolism indicated by [¹⁸F]-FDG-PET (Fig. 2A). The SDM of this patient's ictal MEG located ECDs at the perirolandic area and deep white matter at the bilateral temporal and parietal lobes.

This patient underwent long-term intracranial EEG monitoring with subdural electrodes at the age of 15. Interictally, spikes were seen over the precentral and postcentral gyri, and ictal ECoG also revealed ictal onset zone at the precentral and postcentral gyri, corresponding to the ictal high-magnitude area of rhythmic activity assessed by STFT and spike sources estimated by SDM. His ictal ECoG was captured 10 times, showing a HFO of >200 Hz intermittently at the supplementary motor area in the pre-ictal period that disappeared in the ictal period. The ECoG also detected the earliest activity in the primary motor area. We therefore proposed that the ictogenesis was located near the primary motor area, although ictal activity indicated bilateral propagation on MEG. Since the ictogenesis was supposed to be in the eloquent area in this case, the patient underwent only partial resection at the primary motor area. His seizures gradually decreased and disappeared completely within 1 year.

Case 3

Interictal EEG showed right central and parietal spikes. Interictal MEG showed clustered spike sources at the right postcentral gyrus by SDM (Fig. 3A). In the first seizure, the ictal EEG demonstrated bilateral frontal and central dominant 12–15-Hz polyspikes. In the second seizure, the ictal EEG showed right-frontal and temporal dominant 15-Hz polyspikes.

Ictal rhythmic activities were obtained from the first seizure of 4.0 s duration and the second one lasting 2.9 s, prior to the accumulation of ictal motion artifact. STFT showed specific rhythmic activities of 10–20 Hz at magnetological onset in the first seizure and 10–15 Hz in the second seizure. Rhythmic activities in the first seizure were generated from the right parietal and temporal lobes; they promptly propagated to the bilateral parietal and temporal lobes (Fig. 3B). Analysis of the same ictal data by SDM located ECDs in the deep white matter of the right parietal and occipital lobes, indicating no bilateral propagation. In the second seizure, rhythmic activity was also generated from right parietal and temporal lobes, however, propagation was limited to the ipsilateral parietal and temporal lobes (Fig. 3C). Analyzed by SDM located these ECDs in the deep white matter of the right parietal and temporal lobes. Both in two ictal MEG, rhythmic activities originated in the vicinity of the interictal spike sources as estimated by SDM.

Discussion

Frequency analyses to ictal MEG

This study indicated that frequency analyses using STFT to ictal MEG provide information about ictogenesis (cases

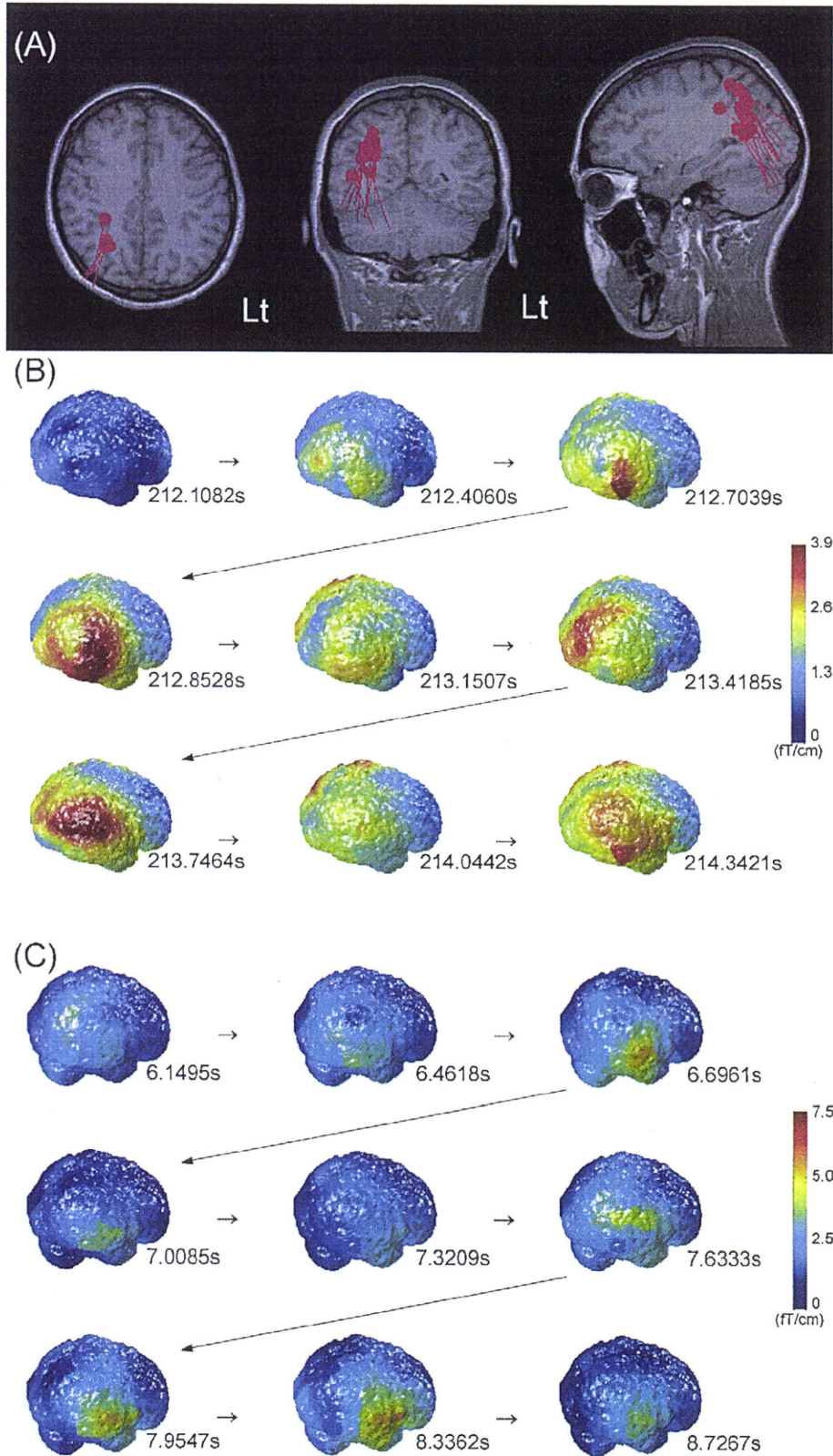


Figure 3 (A) Case 3 SDM: spike sources are clustered at the right postcentral gyrus. (B) Case 3 first seizure 3D-MRI overlay: high-magnitude zone of 10–20 Hz oscillation projected to 3D-MRI. High-magnitude area starts at the right parietal and temporal lobes and promptly propagates to the bilateral temporal and parietal lobes. (C) Case 3 second seizure 3D-MRI overlay: high-magnitude zone of 10–15 Hz oscillation generated from the right parietal and temporal lobes; these propagations were limited.